TNO innovation for life

WAGENINGEN UNIVERSITY & RESEARCH

Slim Landgebruik

Method comparison and implications

Gaseous emissions after renovation of grassland

TNO Intern ⟩ TNO 2023 R11 419
16 January 2024

Energy & Materials Transition
www.tno.nl
+31 88 866 50 65
info@tno.nl

TNO 2023 R11 419 – 16 January 2024

Gaseous emissions after renovation of grassland

Method comparison and implications

Author(s)	I. Velzeboer, P. Wintjen, W.C.M. van den Bulk, D. van Dinther, K.F.A. Frumau, A. Hensen, J.P. van 't Hull, M.B.H. Ros, G.L. Velthof, G. Dorland
Classification report	TNO Intern
Title	TNO Intern
Report text	TNO Intern
Number of pages	55 (excl. front and back cover)
Number of appendices	1
Project name	Gaseous emissions after renovation of grassland
Project number	TNO: 060.48531 WUR: 52000-47404

Samenvatting

Naar aanleiding van het Parijs akkoord en de daaropvolgende Nederlandse klimaatakkoord in 2019 heeft de Nederlandse overheid het doel gesteld om broeikasgasemissies te verminderen van 55% in 2030 en 80-95% in 2050. De landbouw speelt een belangrijke rol in het Nederlandse broeikasgas budget. Het doel is om 3.5 Gg CO_2-equivalenten te reduceren in de landbouw sector per in 2030, waarbij 0.5 Gg CO_2-equivalenten per jaar in de Nederlandse minerale landouwbodems middels koolstofvastlegging. Het doel van het programma 'Slim Landgebruik' is het leveren van de benodigde kennis om te komen tot een additionele vastlegging van 0.5 Mton CO_2-equivalenten per jaar in de Nederlandse minerale landbouwbodems in aanloop en vanaf 2030.

Eén van de kansrijke maatregelen is het *niet* scheuren van grasland vanwege het grote grasland areaal in Nederland. Het onderzoek in dit rapport is erop gericht om inzicht te krijgen in de hoeveelheid koolstof die verloren gaat bij directe herinzaai en het omzetten naar bouwland en de daarbij gepaarde lachgas emissie en tegelijkertijd het vergelijken van verschillende meetmethodieken. De CO_2 en N_2O emissies zijn gemeten op drie naastgelegen velden die onderverdeeld zijn in de behandelingen (i) permanent grasland, (ii) herinzaai en (iii) omzetten naar bouwland (tarwe). De metingen zijn uitgevoerd op drie verschillende manieren: een vernieuwde intermitterend Eddy-Covariance benadering, een fast-box methode en de statische kamermethode. Fluxen van de Eddy-Covariance methode zijn elk halfuur gemoniteerd in elk van de drie velden. De totale netto uitwisseling is verkregen door het berekenen van de cumulative flux over de gehele meetperiode. Voor de fast-box methode is per veld op zes plots gemeten. Voor de kamermethode is per veld op negen plots gemeten. De fluxen zijn gemiddeld 1x per week gemeten, tijdens peak events (scheuren, bemesten, regenval) is 2x per week gemeten.

Uit de resultaten van de eddy-covariance methode komt naar voren dat ploegen resulteert in een verlies van C in de vorm van CO_2 voor zowel herinzaai als conversie naar bouwland. Gedurende de gehele meetperiode heeft bouwland een netto C verlies van 184g C m^{-2} (1.84 ton C ha^{-1}), hetgeen betekent dat conversie naar bouwland een bron van CO_2 is. Daarentegen heeft het ploegen voor herinzaai voor een tijdelijk verlies van C gezorgd, maar door de groei van het nieuwe gras werd koolstof weer opgeslagen. Aan het eind van de meetperiode was de netto exchange gelijk aan -44 g C m^{-2} (0.44 ton C ha^{-1}). Dat maakt herinzaai een kleine C sink. Permanent grasland, ofwel het niet scheuren van grasland, leidt tot een netto exchange van -292 g C m^{-2} (2.92 ton C ha^{-1}). Permanent grasland is daarmee een relatief grote C sink. De cumulatieve N_2O- emissies voor alle drie de methodes verschilden van elkaar en varieerden van 1.1-3.36 N_2O ha^{-1} voor conversie naar bouwland, 1.66-2.67 kg N_2O ha^{-1} voor herinzaai en 0.17-0.86 kg N_2O ha^{-1} voor permanent grasland. De emissie bij permanent grasland was het laagst bij alle drie de meetmethodes, maar voor herinzaai en bouwland waren de resultaten tegenstrijdig. De piek emissies zijn gerelateerd aan management zoals ploegen en bemesting.

Uit de resultaten kan er geconcludeerd worden dat permanent grasland, ofwel het niet scheuren van grasland, de voorkeur heeft boven herinzaai en omzet naar bouwland als het gaat om koolstofopslag. Toch is het scheuren van grasland noodzakelijk vanwege het behoud van voedingswaarde, opbrengst en bodemkwaliteit. Deze studie laat zien dat periodiek scheuren van grasland op de lange termijn niet leidt tot koolstofverlies. Het omzetten van grasland naar bouwland leidt wel tot duidelijk koolstofverlies. De N_2O emissie was het laagst voor permanent grasland waabij alle drie de meetmethodes in overeenstemming waren. Voor herinzaai en bouwland waren er verschillen waarneembaar tussen de verschillende meetmethodes. Desallniettemin heeft permanent grasland de voorkeur in termen van CO_2-equivalenten.

Summary

In line with the Paris Agreement and the Dutch Climate Agreement, the Dutch government has set targets of 55% reduction in 2030 and 80-95% reduction in 2050. Agriculture plays an important role in the Dutch national GHG budget. The aim is to reduce its GHG emissions by 3.5 Gg CO_2-equivalents per year in the agricultural sector by 2030. About 0.5 Gg CO_2-equivalents should be obtained through carbon (C) sequestration in mineral soils. The goal of the Dutch national program 'Smart Landuse' is to acquire the requisite knowledge to achieve the goal of 0.5 Gg CO_2-equivalents sequestration.

One of the promising measures is grassland management due to the substantial area of grassland in the Netherlands. Here, a field experiment was conducted to assess the effect of grassland renewal and conversion to arable land (wheat) on carbon loss and N_2O emission and simultaneously compare various measurement methods. Emissions of CO_2 and N_2O in three adjacent plots (renewed grassland, converted grassland, and permanent grassland) were monitored using a novel intermittent Eddy-Covariance approach, a fast-box method, and a classic static chamber method. Fluxes of the Eddy-Covariance approach were reported every half hour at one of the three fields. The total net exchange is obtained by calculating the cumulative flux over time. The fast-box method and the static chamber method was measured in six and nine replicates per plot, respectively. Fluxes are, on average, reported every week but during certain events (e.g. tillage, fertilization, rainfall) the measurement frequency was increased.

The results of the eddy-covariance approach show the effect of tillage causes a loss of carbon through CO_2 in the first weeks for both the reseeded and the wheat treatment. The wheat field lost carbon during the measurement period leading to a net exchange of 184g C m^{-2} (1.84 tonnes C ha^{-1}) to the atmosphere, making the wheat treatment likely a carbon source. This means that tillage and subsequently transforming grassland to arable land is likely to be a carbon source. For the reseeded treatment, tillage causes a high loss of C in the first weeks as well, but as the new grass started to grow, carbon was taken up. The loss of C in the first weeks was already compensated in August and at the end of the measurement campaign the net C exchange was -44 g C m^{-2} (0.44 tonnes C ha^{-1}). The reseeded treatment therefore appeared to be a small C sink. At the end of the campaign, the reference field took up 292 g C m^{-2} (2.92 tonnes C ha^{-1}), making the reference treatment a relatively big C sink. In terms of nitrogen, the cumulative emissions throughout all three methods varied ranged from 1.1-3.36 kg N_2O ha^{-1} for wheat, 1.66-2.67 kg N_2O ha^{-1} for reseeded and 0.17-0.86 kg N_2O ha^{-1} for the reference treatment. The emission for permanent grassland was lowest for all methods, but for reseeding and conversion to arable the results were conflicting. Peak emissions were related to tillage and fertilization.

In terms of carbon storage and climate mitigation, we conclude that permanent grassland would be the preferred option over conversion to arable land and grassland renewal as permanent grassland was a sink for carbon. However, grassland renewal is considered important to maintain the yield and nutritional value of the grass, as well as to keep up other ecosystem services related to grass production, such as soil quality. This study show that periodical grassland renewal does not lead to C loss at the end of the experimental period. On the contrary, conversion to arable land result in a net C loss. N_2O- emission was lowest for reference overall, but for reseeded and wheat the results are not in agreement throughout all three methods. Nevertheless, in terms of CO_2-eq, permanent grassland is the preferred option over grassland renewal and conversion to arable land.

Contents

1 Introduction

In the COP climate meeting in Glasgow in 2021 the call to respond to a changing climate was very clear. Mitigating climate change will be one of the major challenges in the decades to come. The role of anthropogenic greenhouse gas (GHG) emissions as the most important driver for climate change was reaffirmed in the sixth assessment report of the IPCC. Substantial reductions of GHG emissions are needed to reduce global warming. In the EU, the ambition is to reduce GHG emission by 40% in 2030 (in carbon dioxide (CO_2)-equivalents, compared to 1990 emission levels) as stated in the Paris Climate Agreement. The Dutch government has set targets of 55% reduction in 2030 and 80-95% reduction in 2050. Agriculture plays an important role in the Dutch national GHG budget, and an important role in that sector is for gases like nitrous oxide (N_2O) and methane (CH_4). The aim is to reduce its GHG emissions by 3.5 Gg CO_2-equivalents per year in the agricultural sector by 2030. About 0.5 Gg CO_2-equivalents should be obtained through carbon (C) sequestration in mineral soils.

The role of grasslands as potential carbon (C) sink is relevant because of the substantial area of grassland in the Netherlands (ca. 10^6 ha). The CO_2 sink can in principle be increased by land management. When doing that it is crucial to understand the impact of the management measures on the carbon (C) and nitrogen (N) cycles. Managed grasslands are known to release substantial emissions of nitrous oxide (N_2O). Since 1 kg of N_2O is equivalent to around 273 kg of CO_2 in terms of global warming according to sixth assessment report of the IPCC, these emissions also need proper quantification. Grassland renovation through ploughing and reseeding is expected to increase both N_2O and CO_2 emissions. The aim of this study is to provide measured data that can help to better understand that process. With that knowledge, we can work towards decreasing N_2O emissions by improved nutrient management. This question is dealt with in the Dutch national program “Smart Landuse” organized by the ministry of agriculture (LNV) in the Netherlands that funded this research project.

The quantification of net ecosystem exchange for CO_2 is well developed by now and the methodology to do that is coordinated on a European scale in the Integrated Carbon Observation System (ICOS) ecosystem research infrastructure. In the protocols on how to measure CO_2 exchange build upon 3 decades of European projects. The procedures for N_2O still need further development. Instruments that can measure N_2O at sufficient accuracy have become available in the recent 5-10 years and are now finding their way to the research institutes all over Europe. The N_2O measurement systems are still a factor 5 more expensive than comparable CO_2 measurement systems and therefore we try to find options to do multiple field measurements while using only one N_2O measurement system.

Here, a field experiment was conducted to assess the effect of grassland renewal and conversion to arable land carbon loss and N_2O emission and simultaneously compare various measurement methods. Emissions of CO_2, and N_2O in three adjacent plots (renewed grassland, converted grassland, and permanent grassland) were monitored using a novel intermittent Eddy-Covariance approach, a fast-box method, and a classic static chamber method. The Eddy-Covariance measurements took place in the three centers of each plot using a sonic anemometer to measure horizontal and vertical wind movements and an inlet line leading to the trailer with the GHG measurement device. From these data, the ecosystem exchange was calculated using the Eddy-Covariance method. Fluxes are reported every half hour at one of

the three fields. The total net exchange is obtained by calculating the cumulative flux over time. The fast-box method and the static chamber method was measured in six and nine replicates per plot respectively. Fluxes are, on average, reported every week but during certain events (e.g. tillage, fertilization, rainfall) the measurement frequency was increased. The effect of grassland management on greenhouse gas emissions and the potential for carbon sequestration was investigated as well as the differences between the measurement methods and their suitability for monitoring greenhouse gas fluxes from grasslands.

Acknowledgements
Unifarm colleagues: Gerard Derks, John van der Lippe and Andries Siepel
TNO colleagues: Jan-Pieter Lollinga, Marcel Moerman, Gerard de Jong and Jun Zhang

Background
In the Dutch Climate Accord of 2019, carbon sequestration one of the measures that the Dutch government wants to implement to reduce greenhouse gas emissions. The goal of the national program 'Smart Landuse' is to provide sufficient knowledge to sequester an additional 0.5 Mton CO_2-eq per year on Dutch agricultural mineral soils from 2030 onwards. Potential measures are identified by Slier et al. (2021), one of them being grassland management (permanent grassland). This measure has the highest potential to sequester C due to its large area of grassland in the Netherlands. However, to identify the realistic potential of this measure it is necessary to quantify the effect on nitrous oxide emission, which is also a greenhouse gas. Therefore, this project aims to quantify the effect no grassland renovation on the CO_2 and N_2O- emission.

2 Material and methods

2.1 Site description

Measurements with a novel intermitted Eddy-Covariance approach, a fast-box method and a static chamber method was carried out on a managed biological grassland with clover with field on a sandy soil in Bennekom (51°59'30.94" N; 5°40'29.70" E). The grassland have been extensively managed with fertilization with cattle slurry from 2012 onwards. Figure 1 and 2 shows an aerial picture of the site and the experimental set-up of the three treatments. The area of the fields are 1.0, 1.0 and 1.66 ha, for wheat, reseeded and reference, respectively.

Figure 1: Site location in Bennekom.

Figure 2: Experimental set-up of the three field: reseeded (blue), wheat (orange) and reference (black) treatment.

The Eddy-Covariance, fast-box and static chamber measurements were carried out during the period April 2021 – December 2021. The monthly precipitation and monthly average temperature (Table 1) were derived from stations of Royal Netherlands Meteorological Institute (KNMI). The highest emission were expected in the period April-September, because this is the period in which N fertilizer is applied to grassland. May 2021, August 2021 and October 2021 were relatively wet in relation to the 30-year average.

Table 1: Monthly precipitation (measured in Wageningen) and average temperature (measured in Deelen) (KNMI)

Month	Precipitation (mm)		Temperature (°C)	
	2021	1990-2020 average	2021	1990-2020 average
January	90	76	3.4	3.7
February	48	66	4.3	4.0
March	44	63	6.4	6.5
April	39	44	6.7	9.8
May	100	63	11.2	13.4
June	74	68	18.2	16.1
July	116	86	18.0	18.2
August	105	86	16.9	17.9
September	24	72	15.9	14.7
October	93	73	11.6	11.0
November	75	78	7.4	7.0
December	79	90	5.4	4.2
Total	886	864		

Soil properties are shown in Table 2.

Table 2: Soil properties of all three fields

Organic matter (%)	3.6
C-organic (%)	1.8
pH (-)	5.2
Clay (%)	2
Silt (%)	11
Sand (%)	83
CEC (%)	95
C/N ratio (-)	12

2.2 Experimental set-up

2.2.1 Planning events and manure application

Cattle slurry (biological) was applied on all three treatments. The N application rate were 50, 50 and 170 kg N per ha per year, for wheat, reseeded and reference treatment, respectively. For the reference treatment, the N appliation was split into three dressings. During the measurement period, several field activities have been conducted. The timing of manure application and field activities are listed in Table 3. Manure analysis is presented in Table 4. For the manure application is it assumed that the composition of the manure is equal for all manure applications.

Table 3 Planning events and manure application.

Event date	Wheat	Reseeded	Reference
20 April	Grass	Grass	Grass
28 April	Start measurement Zero measurement	Start measurement Zero measurement	Start measurement Zero measurement
3 May	Mowing Tillage Manure application: 50 kg N	Mowing Tillage	Mowing Manure application: 50 kg N
6 May	Ploughing sowing	Ploughing sowing	
7 June	Mechanical weed control		
14 June	Mechanical weed control		Mowing
17 June			Manure application: 70 kg N
9 August	Harvest		Mowing
12 August	Sowing	Manure application: 50 kg N	Manure application: 50 kg N

Table 4: Composition of cattle slurry applied throughout the experiment. For the manure application is it assumed that the composition of the manure is equal for all manure applications.

Dry matter (g DM kg^{-1})	110
Organic matter (g OM kg^{-1})	79
Nitrogen (g N kg^{-1})	3.95
C/N ratio (-)	9

2.2.2 Canopy heights

Canopy height was estimated during days of field activities (see Table 5), e.g. fertilizing, ploughing, mowing, etc. Canopy height was measured at several places in the fields to determine an average height. According to the EddyPro software, roughness length, and displacement height were obtained by multiplying canopy height with 0.15 and 0.67, respectively. Dynamic canopy heights during the campaign period were interpolated for each individual period.

Table 5: Estimated canopy heights of each field (W = wheat, RS = reseeded, RF = reference) during the measurement campaign. Displacement height and roughness length were calculated as 0.67 times canopy height and 0.15 times canopy height, respectively.

	Canopy height [m]			Displacement height [m]			Roughness length [m]		
Day	W	RS	RF	W	RS	RF	W	RS	RF
28 April	0.1			0.067			0.015		
3 May	0.05			0.0335			0.0075		
6 May	0.01			0.0067			0.0015		
4 June	0.1	-	-	0.067	-	-	0.015	-	-
13 June	-	-	0.3	-	-	0.201	-	-	0.045
14 June	0.2	0.1	0.05	0.134	0.067	0.0335	0.03	0.015	0.0075
8 July	0.3	0.25	0.2	0.201	0.1675	0.134	0.045	0.0375	0.03
9 August	0.5	0.4	0.2	0.335	0.268	0.134	0.075	0.06	0.03
13 August	0.01	0.05		0.0067	0.0335		0.0015	0.0075	
29 October	0.5	0.2	0.15	0.335	0.134	0.1005	0.075	0.03	0.225

2.2.3 Soil and plant analysis

The aboveground biomass of the grassland treatments was harvested (three cuts) with an Haldrup harvester, from a representative area of 10-12 m^2 for each plot. To determine the total dry matter (DM), sub samples of plant material were dried at 105 °C for 24 hours. Total nitrogen (Nt) analyses was performed at the Soil Chemistry Laboratory (CBLB) in Wageningen.

Soil samples were taken from each treatment the 20th of April 2021 (before the experiment started) to determine the soil characteristics. These are shown in Table 2. NIR analyses was performed at Eurofins Agro in Wageningen.

Soil samples for determinining the mineral nitrogen (N_{min}) dymanics during the measurement period were taken weekly for each treatment from 0-10cm with a gouge auger with an inner diameter of 2 cm. A composite sample was taken from 20 per treatment each. The samples for both soil characteristics and mineral N were taken evenly across the field by walking zigzagging through the field. Each time, approximately 1kg of soil was collected.

2.2.4 Additional analyses

The soil temperature and soil moisture was only collected at the Bennekom and Wageningen site at a depth of 0-11cm using a digital soil probe with (Gropoint Lite, Riot Technology, Canada) at an hourly time interval. In addition, air temperature was collected from the Royal Netherlands Meterological Institute (KNMI; De Bilt) and precipitation from the KNMI weather station in Wageningen.

2.3 Gaseous measurements

2.3.1 Static chamber method

Additional chamber measurements were performed with a PICARRO G2508 cavity ring-down spectroscopy gas analyzer (PICARRO, USA). Figure 3 shows the experimental set-up of these measurements. For each treatment there were nine plots with approximately 20 meter in between.

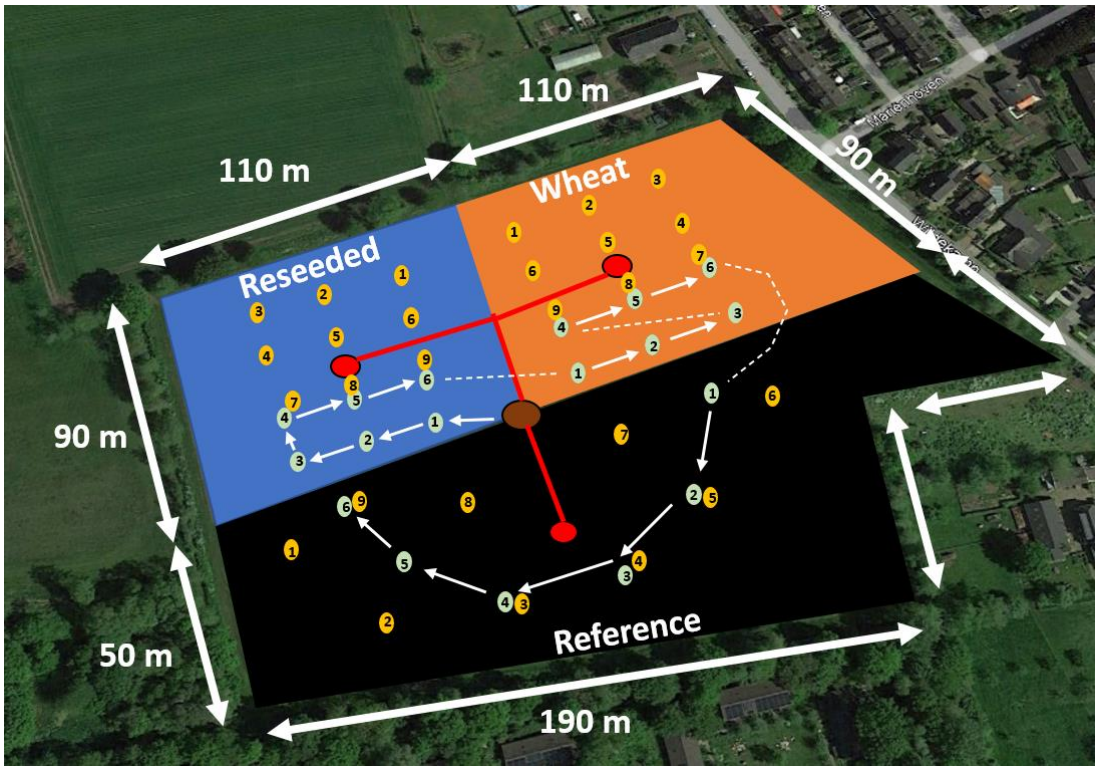

Figure 3: Experimental set-up for the static chamber method (yellow), fast-box method (light green) and eddy-covariance (brown and red).

N_2O fluxes were measured weekly from April 2021 to November 2021. The measurements were performed with the closed chamber method (Oertel et al., 2016). The sampling started before renovation, and the sampling frequency was on average once per week during growth season, but it was increased during the first week after grassland renewal, conversion and after N application. Outside the growth season, the frequency decreased to once per month on average. This results in an average of 24 measurements during the measuring period. At the beginning of each experimental year, a PVC collar of 20 cm diameter and 10 cm height was installed permanently into the soil to a depth of 5 cm at the centre of each plot to provide a base for the measurements (Hutchinson & Mosier, 1981). These collars were only removed during renovation, harvesting and N application for a short period of time and were afterwards installed on exactly the same place. During N_2O measurements, gas-tight chambers with a height of 23.5 cm were placed on top of these collars to create a closed system of 4.7 L chamber volume (Figure 4). To allow gas sampling during measurements, the chambers were equipped with a rubber septum and vent tubes on the top.

Figure 4: Installed pvc collar as a base of the chamber measurements (figure left) and a gas-tight chamber on top of the collar (figure right).

After the chambers were placed on top of the collar, gas samples were taken after 10 minutes. The N_2O fluxes were then calculated using linear regression. Linear increase of the gas concentration was weekly tested during the whole measurement period on 1-2 random samples by measuring 15 minutes continuously. On average, the increase was very linear (R^2 = 0.99) and therefore it was assumed that the concentration in all samples increased linearly over the 15 minute closure period (Figure 5). Examples of Static chamber measurements on the reseeded field and the wheat field are shown in Figure 6.

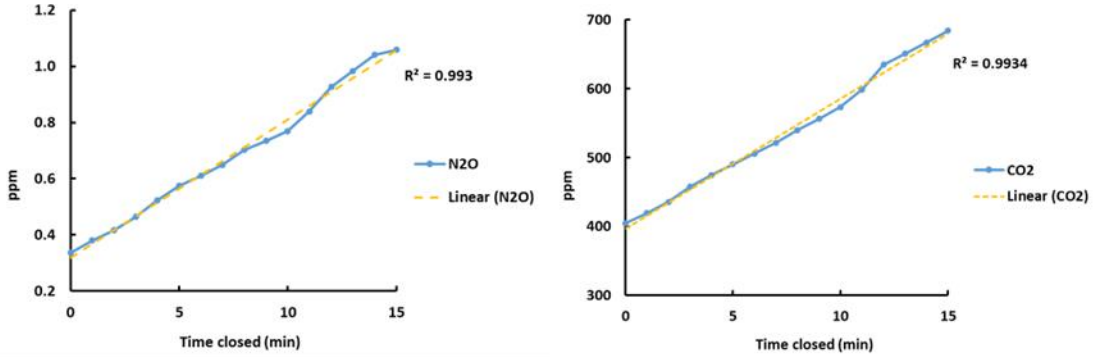

Figure 5: Continuous measurements for N_2O and CO_2.

After the measurements were finished, the flux was then calculated as followed:

$$Flux = \frac{(C_t - C_a) * m_{N2O} * \beta * V}{\Delta t * V_m * A} \qquad (\mu g\ N - N_2O\ hour^{-1} m^{-2}) \qquad (1)$$

The flux per squared meter is the difference between de N_2O concentration (C_t in µL/L) at time of measuring and the N_2O concentration at the moment of closing the chamber (C_0 in µL/L) multiplied by the volume of the chamber (V), the molar mass (m_{N2O} = 44 gram) and a conversion factor (β = 28/44) to calculate N_2O-N, and then divided by the closure time (Δt in hour), the volume of the chamber (V) and the area of the chamber (A). Flux rates were expressed as the mean (n = 9) with the standard deviation of the replicated plots. The accumulated annual N_2O-N emission was calculated by linear interpolation between the measured daily fluxes.

Figure 6: Static chamber measurements on reseeded (upper figure) and wheat (lower figure).

2.3.1.1 Statistical analyses

Statistical analysis was performed using IBM SPSS Statistics 25 (IBM Corp, 2017). An analysis of variance (ANOVA) was conducted to analyze the effects of the treatments and year on the soil mineral N samples and on the cumulative N_2O- fluxes. Where ANOVA indicated the differences, a Tukey's HSD test was used as a post hoc evaluation for comparisons of all the tests. The normality of the residuals and variance homogeneity was checked prior the analyses to meet the requirements of these tests. In case the residuals were not normal, the data was log transformed.

2.3.2 Fast-box chamber measurements

Figure 7 shows a typical design of chamber placed at six positions on each field within the flux footprint shown in Figure 3. Depending on the vegetation height, the box volume was adjusted (small, middle, large), with volumes of 157, 320 and 605 L (dimension: 0.8 m x 0.8 m x 0.245 or 0.5 or 0.945 m). CO_2 and N_2O were sampled in weekly intervals during the measurement campaign and numbers in Figure 3 indicate the measurement order. A vent system was installed inside the chambers to ensure sufficient gas mixing.

Figure 7: Set-up for fast-box chamber measurements.

Exposure duration of the chambers was 1-5 minutes depending on the magnitude of the flux. For high flux conditions, 30 seconds of measurements were sufficient, for low emissions a longer accumulation time is used. Each second concentration data was obtained. The flux corresponds to the slope determined by a linear regression on concentration data (Velthof, G. and Oenema, O., 1995; Velthof et al., 1996). Finally, the flux is calculated as followed:

$$F_{chamber} = sl_{conc} \cdot {}^{M_{gas}}/_{V_m} \cdot h \qquad (2)$$

where, F_{camber} is chamber measured flux (in µg N_2O m^{-2} s^{-1}); sl_{conc} is the slope of concentrations during the sampling period (in ppb s^{-1}); M_{gas} is molar mass of the gas considered, 44 g mol^{-1} for CO_2 and N_2O. V_m is the molar volume (in L mol^{-1}); h is the height of the box above the ground surface (in m).

For an emission per m^2 the horizontal dimensions of the box cancel in the equation. The size of the box does matter in terms of the area for which the measurement is truly representative. Especially for N_2O hotspots occur in the soil, therefore it is important to measure at multiple locations within one field and average these data.

A proper quality criterion is the squared correlation coefficient obtained from linear regression analysis. For reducing uncertainty, the average of the chamber fluxes was taken.

2.3.3 Eddy Covariance

2.3.3.1 Set-up

Instrument installation took place at the Wageningen University agricultural research site on 25 April 2021, and data recording started 3 days later. The research area was separated into 3 fields. Summer wheat and grass were seeded on field west (wheat; W) and east (reseeded; RS), respectively, and on field south (reference; RF), no grassland renewal was made (Figure 2). Site instrumentation was dissembled at 29 October whereas measurements at field W and RS stopped already at 21 October. On field W and RS, a sonic anemometer (GILL Windmaster

Pro, Gill Instruments, Lymington, UK) was positioned in the centre being ca. 40 m and 50 m distant to the lower and left field border. The same sonic was placed 25 m in a straight line from the trailer on field RF. The distance was reduced to 13 m from the 17 June onwards. All sonic anemometers were approximately 1.9 m above ground and had the firmware version (2329-701). The inlets (see Figure 8 right) via at least 90 m long, opaque sample lines to a dual-laser spectrometer (Aerodyne TDLAS, Billerica, MA, USA) measuring the trace gases CO_2, N_2O, water vapor (H_2O), CH_4, ethane (C_2H_6), and carbon monoxide (CO) with a sampling frequency of 5 Hz.

Measurements of spectral lines were done in a 78 m multi-pass cell of 0.5 L at 30 Torr (*ca.* 4 Kpa). To ensure the low pressure inside the sample cell and keeping laser performance temperature stable, a dry vacuum scroll pump and peltier cooler were connected to the lasers leading to flow rates of ca. 5 L min^{-1} and laser temperatures of 12.60°C for measuring CH_4, C_2H_6, and H_2O and 8.46°C for measuring CO_2, N_2O, and CO. The laser spectrometer, pump and peltier cooler were housed in an air-conditioned trailer. Further specifications to the site setup are given in Supporting Table S1.

With a valve system (Figure 8), the three fields were measured by switching between the fields every 30 minutes. Sonic temperature and wind components were recorded continuously with 20 Hz. Calibrations of the laser spectrometer were performed on a regular basis, on average once every week with field calibration flasks that were linked to the ICOS CO_2, CH_4, N_2O levels by an intercomparison of the flask air with the standards obtained from the ICOS calibration centre in Jena.

Sonic and laser spectrometer data were jointly stored in Eddycor (program developed at ECN), and data from the laser spectrometer were additionally stored in a “meetwagenprogramma”. In this way, the incoming laser spectrometer data was shown directly on the screen. It was stored as a CSV file, and during the measurements, field notes were taken, for example to add when chamber-measurements took place, or activities on the field. After processing, the Eddycor program provided CSV files per day including the sonic and laser spectrometer data.

Finally, a MatLab script was used to link the right sonic data to each concentration measurement. Resulting files were stored in half-hourly time intervals. Micrometeorological data of temperature, relative humidity, and atmospheric pressure were provided by the weather station at Veenkampen (51.98 N, 5.62 E, 9 m a.s.l., ca. 4 km away from the experiment field) hosted by the University of Wageningen. These data were used to correct for drifts in sonic temperature and for water vapor in ambient air. Soil water volume and soil temperature of each field were measured at the uppermost soil layer (0-7 cm). Short wave incoming radiation and boundary layer height were downloaded from the Copernicus Climate Data Store (CDS) (https://cds.climate.copernicus.eu/cdsapp#!/dataset/reanalysis-era5-single-levels, last access: 20 May 2022). Micrometeorological and soil data were used to perform the flux gap-filling.

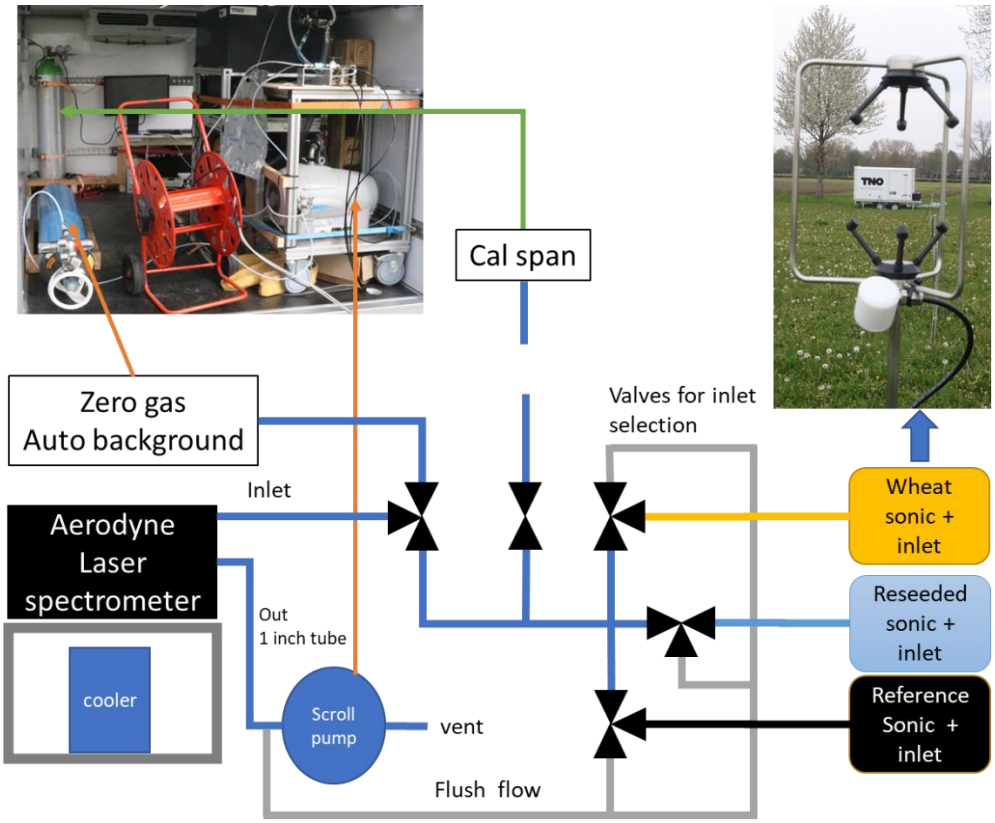

Figure 8: Instrument set-up and valve scheme; top left: Laser spectrometer and valve set-up in trailer; bottom left: valve schedule; top right: sonic with inlet.

2.3.3.2 Eddy Covariance measurements

Trace gas fluxes were calculated using the Eddy-Covariance (Aubinet et al., 2012; Burba, 2013) (EC) method. Basically, the covariance is calculated by shifting the time series of vertical wind and concentration against each other until their covariance is at maximum. The various gas sampling delay times were due to different lengths of inlet lines per field. Time lags were around 12 s for Field W and Field RS in the north and 12 s until 16th June switching to 4 s after reducing sample line length for Field RF. Later on, the half-hourly flux data were calculated by using the open-source software EddyPro (Licor Biogeosciences, 2019, version 7.0.6).

Before flux calculation is allowed, several assessments on raw data timeseries have to be made. At first, EddyPro was instructed to remove spikes from raw data timeseries and to replace occurring gaps by linear interpolation according to Vickers and Mahrt (1997). An angle-of-attack correction (Nakai and Shimoyama, 2012) and a subsequent (double) coordinate rotation (2D) (Wilczak et al., 2001) was made on measured wind speed components. The first is needed due to flow distortion by the sonic frame, the latter is mandatory in EC flux calculations for eliminating the respective mean wind component. A trend removal, a subtraction of the mean from raw time series (block average), was made at last. For calculating the covariances, the option 'covariance maximization with default' was chosen, thereby instructing EddyPro to search for the maximum covariance, the flux, in a predefined range of possible time lags. If no covariance maximization was possible in that range, EddyPro provided the flux for the default time lag.

To evaluate the quality of the obtained fluxes, the flagging policy of Mauder and Foken (2006) was chosen, based on a stationarity test of the covariances for small intervals compared to the measurement interval and on the integral turbulence characteristics test proving if the ratio of standard deviation and its flux is a function of stability. For detecting fluxes related to insufficient turbulence, half-hours with friction velocities (u_*) below 0.1 m s^{-1} were not considered in analysis. Absolute flux limits, namely -300 to 200 µg C m^{-2} s^{-1} and -50 to 250 ng N m^{-2} s^{-1} for CO_2 and N_2O, respectively, were defined for removing outliers. Ranges were set based on visual screening. Random flux error was calculated following Finkelstein and Sims (2001). Fluxes were corrected for low-frequency damping artifacts (Moncrieff et al., 2004), which are mainly caused by the selected detrending method. For determining the high-frequency flux losses, we compared the results of a theoretical method and a recently developed empirical method by Wintjen et al. (2020). Further details to that decision are given below.

2.3.3.3 Corrections for long inlet lines – Damping

The measured vertical fluxes using EC method hold contributions of small and large-scale eddies occurring at high frequencies (> 1 Hz) and low frequencies (> several minutes). Due to limitations of the instruments in response time, sampling rate, the physical dimensions of the analyzing cell, the position of the inlet to the sonic anemometer, and distance to the analyzer, not all eddies could sufficiently be detected.

To visualize the ability of the EC setup to capture the eddies contributing to the flux, a cospectrum of the vertical gas flux is calculated from measured raw time series of concentrations and vertical wind (Figure 9 and Figure 10). Usually, the gas flux cospectra are compared to cospectra of sensible heat or theoretical turbulence spectra to identify the frequencies (eddies) which are missing in the gas flux. Low-frequency flux losses are caused by the finite time averaging and flux pre-processing options like the chosen detrending method. Low-frequency flux losses are generally in the order of a few percent and treated equally for various chemical compounds. The high-frequency flux losses are more complex and differ significantly for the type of analyzer and the desired compound. In case of closed-path instruments, inert compounds like CO_2 show fluxes losses are generally between 5% to 15%, whereas more sticky, reactive compounds like H_2O have flux losses up to 40% (Su et al., 2004; Ibrom et al., 2007; Mammarella et al., 2009).
Fortunately, there are several methods developed estimating high-frequency flux losses and even integrated in modern flux processing software like EddyPro. This software offers the commonly used Moncrieff et al. (1997) for correcting measured fluxes. This method describes occurred damping processes theoretically and uses theoretical turbulence spectra. The flux damping is simulated by spectral transfer functions (Moore, 1986), which depend only on the measured physical dimensions of the setup and the response time of the analyzer, and flux measurements themselves are not needed for this method.

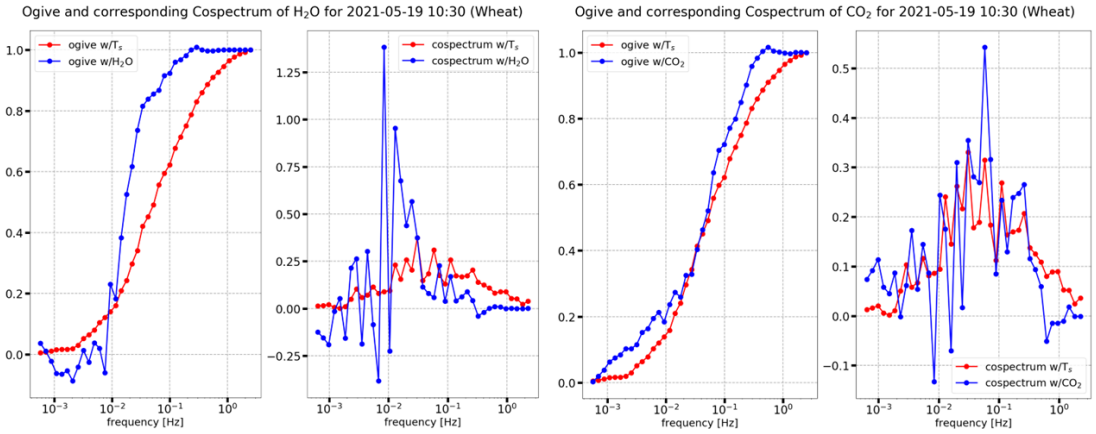

Figure 9 Ogive and cospectra of H_2O (left,blue) and CO_2 (right, blue) for a certain half-hourly flux for the wheat field. Sensible heat ogive and cospectra are coloured red. Spectral data were binned into log-spaced frequency data points.

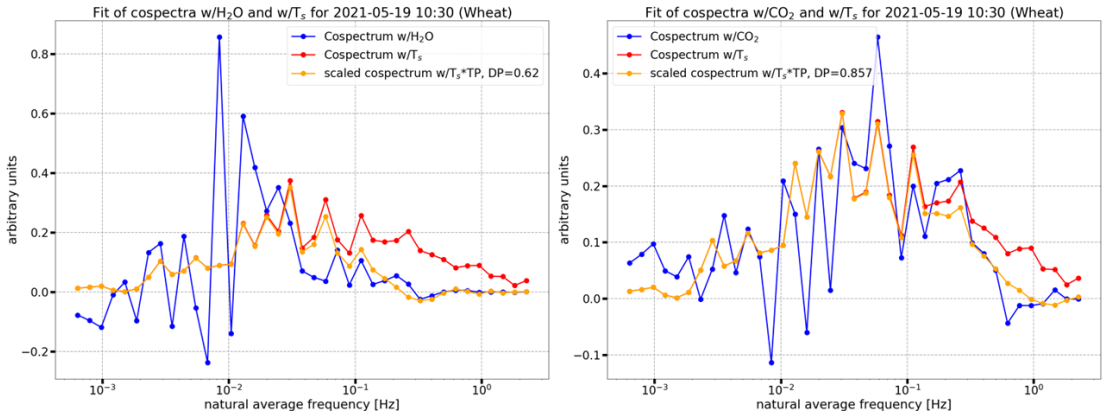

Figure 10: Half-hourly cospectral fit according to the ICO method (Wintjen, et al., 2020) of H_2O (left) and CO_2 (right) for the wheat field. Damping factors of 0.62 and 0.86 were calculated for H_2O and CO_2, respectively.

Theoretical approaches for correcting high-frequency flux losses may not be suitable for the installed EC setup due to the long inlet lines. Thus, we adapted the empirical approach based on measured cospectra recently published by Wintjen et al. (2020) called in-situ cospectral method (ICO). We used their suggested transfer function (Eq. 3 of Wintjen et al. (2020) and set 0.1 Hz as lower frequency and 2.5 Hz as upper (maximum) frequency for the non-linear fit. Further details to the theoretical and empirical approach can be found in their respective publications. Figure 9 and Figure 10 show an example of CO_2 and H_2O using the ICO method for damping estimation. A similar picture for N_2O can be found in the appendix (Supporting Figure S2). Generally, H_2O had the largest flux loss in the high-frequency range, and similar flux losses were found for CO_2 and N_2O. The example for N_2O refers to high flux conditions, which were caused by a recent manure application.

Fluxes were multiplied with median correction values, which have weekly and biweekly time resolution intervals. Approximately, 52% of valid damping factors were left for each two-week period. An aggregation of damping factors was made due to a generally limited amount of valid correction factors. We further applied the following quality selection criteria to half-hourly damping values: consider only QC=0 according to flux selection criteria by Mauder and

Foken (2006) (i), remove cases of insufficient turbulence ($u_* < 0.1$ m s^{-1}) (ii) and if half-hourly concentration variance was larger than the campaign average plus its standard deviation times two (iii), and choose only half hourly gas fluxes with a measured time lag (iv).

2.3.4 Cumulative fluxes and comparison with chamber measurements

The sequential measuring on each field can cause at least 1/3 of data gaps in the entire period. In addition, instrument outages, and quality filtering of EC fluxes led to extra gaps in flux time series as well. To estimate the total carbon and nitrogen uptake, which is essential for evaluating applied land management strategies, missing values have to be generated by gap-filling approaches. For CO_2, we used the marginal distribution sampling technique (Reichstein et al., 2005) implemented in the online gap-filling tool REddyProc (Wutzler et al., 2018) hosted by the Max-Planck Institute for Biogeochemistry. This approach is optimized for CO_2, latent, and sensible heat fluxes. For using the online tool, fluxes and additional micrometeorological variables were merged into a file, which was uploaded to the website. Unfortunately, the application of a u_* threshold detection algorithm was not possible due to the low number of valid half-hourly fluxes. For N_2O, this method is not suitable due to the low auto-correlation of the N_2O flux pattern. Thus, we used a combination of different gap-filling approaches. We used the novel gap-filling approach based on a random forest algorithm (Mahabbati et al., 2021; Zhu et al., 2022) implemented in Phytons' scikit-learn package (Pedregosa et al., 2011).

Based on 1000 decision trees with unlimited leaves, flux predictions are made on a trained dataset set. The input parameters used for flux prediction were N_2O concentration, global radiation, friction velocity (u_*), wind direction, top soil water volume, and soil temperature. Apart from soil water volume and soil temperature, all other input parameters based on measured data.

Since the sonic anemometers are close to their respective field border (approx. 40 m), flux footprints have substantial contributions from the other fields or even from urban settlement or neighbouring grasslands and gardens depending on the wind direction and stability. The influence of the outer area is not fully known, but the contribution of the inner field areas can be approximated by their gap-filled fluxes. For footprint calculation, we used the model by Klijun et al. (2015). We implemented their code in a PYTHON script, which calculates the contribution of all fields to the 80% footprint aera.

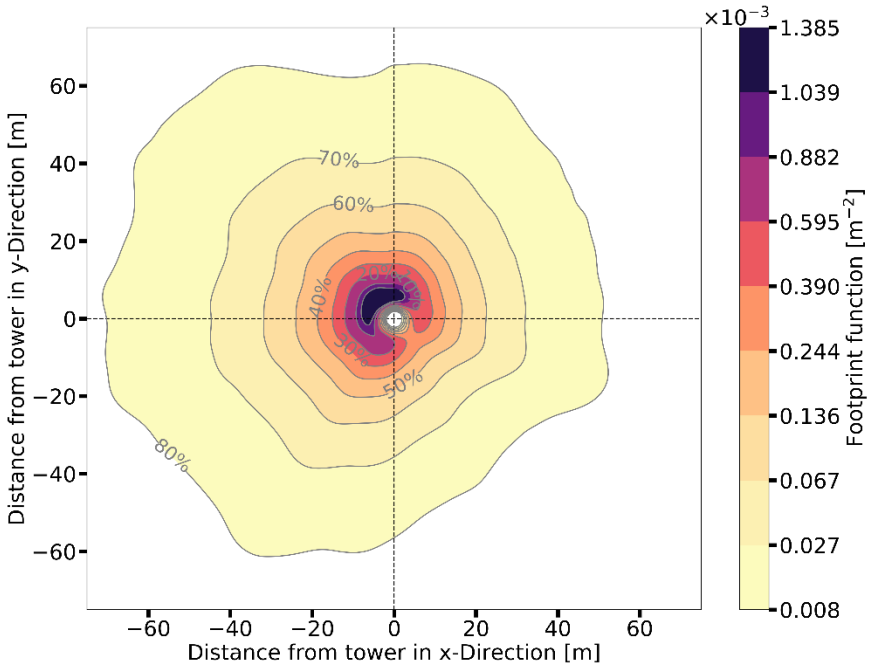

Figure 11: 2D footprint analysis of the wheat field. Lines ranging from 10 to 80 % show the contribution of certain aeras to the total flux. The heatmap shows from which wind direction most of the flux is originating. Please note that the heatmap represent the entire campaign.

We took the 80% as reference following the ICOS recommendations for flux evaluation (Rebman et al., 2018; Figure 11). Monthly averages of specific half hour values of the reference field were used as approximation for the flux of the outer areas (F_{out}). That is likely reasonable for CO_2. In case of N_2O, we assume that fluxes in the outer area are zero. To take the contributions of the surroundings into account, an aera weighted flux was calculated as follows: For each 90° wind direction sector, three equations were defined in order to calculate the flux of the individual fields f_{Win}, f_{RSin} and f_{RFin}. Here, the three governing equations for wind directions from 0° to 90° are shown as example.

$$f_{Win} = \left(F_{WG} - F_{\text{out}} \cdot a_{W\_\text{out}}\right)/a_{W\_W}$$
$$f_{RSin} = \left(F_{RSG} - f_{RS} \cdot a_{RS\_W} - F_{\text{out}} \cdot a_{RS\_\text{out}}\right)/a_{RS\_RS}$$
$$f_{RFin} = \left(F_{RFG} - f_{RF} \cdot a_{RF\_W} - f_{RS} \cdot a_{RF\_RS}\right)/a_{RF\_RF} \quad (3)$$

The measured half-hourly flux of the total footprint area is defined as FWG, FRSG, and FRFG, and the area contributions as ax_y where x defines the field of the total footprint and y the field contributing to the total footprint. The weights of the individual fields aW_W, aRS_RS, and aRF_RF can be close to zero under certain circumstances leading to unreasonably high flux values. Thus, if these area weights are less than 5%, individual field fluxes are set to not a number (nan). Figure 12 illustrates the footprint coverage for the selected wind direction 0° to 90°. The slight south east orientation of the reference field was not considered in this approximation.

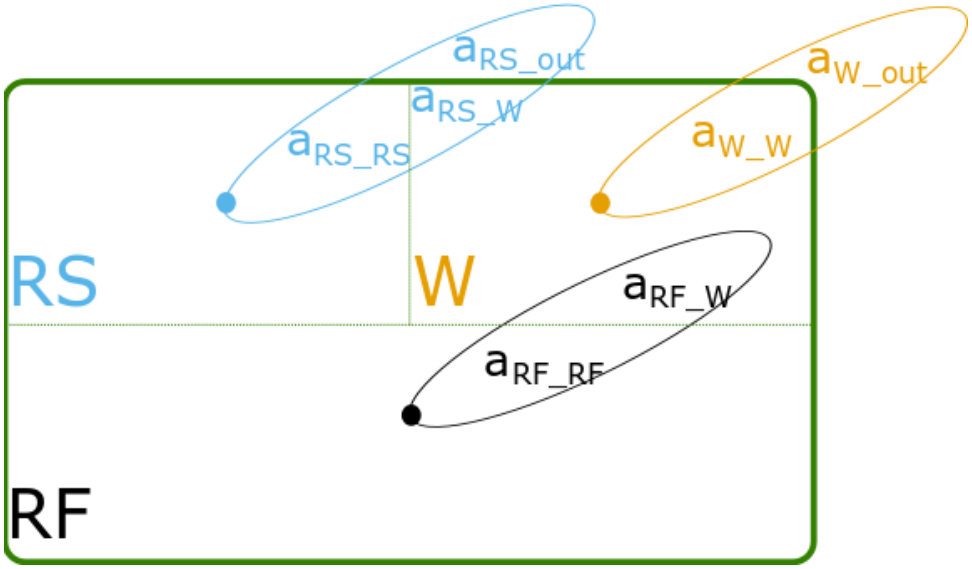

Figure 12: Schematic sketch of the footprint coverage for each field if wind is coming from 0° to 90.

3 Results and discussion

3.1 Additional analyses

3.1.1 Soil analysis

Figure 13 presents the soil mineral N content over time for all three treatments. The dotted orange line represents the timing of tillage and manure application. Before tillage and manure application was done the soil mineral N varies little from 25 to 31 mg/kg. On the 3th of May tillage was performed and manure was applied. This has increased the soil mineral N slightly for wheat and reference treatments. For reseeded however, tillage was performed and no manure was applied. This did not lead to increased soil mineral N. Manure was again applied on 17th of June on the reference treatment and again applied on 12th of August for both reference and reseeded. The soil mineral N content increased in the weeks after manure application.

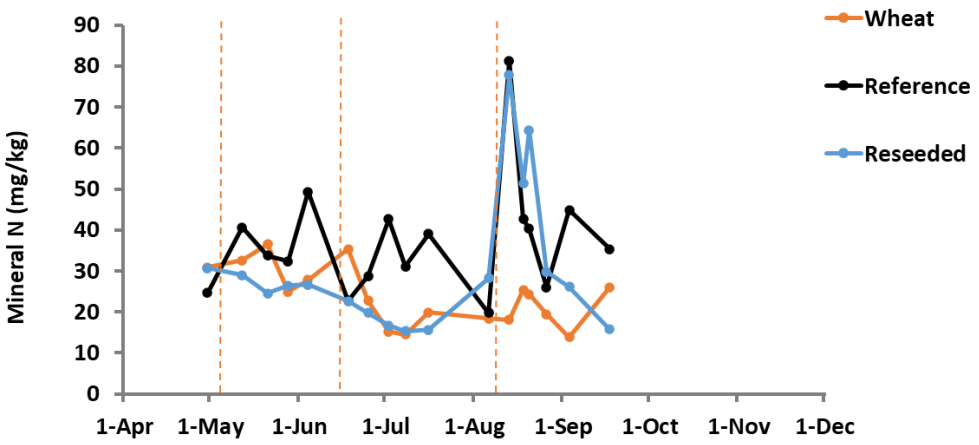

Figure 13: Soil mineral N dynamic over time during the measurement period.

3.1.2 Yield

The yield of the treatments were 82, 118 and 120 kg N for the reference treatment, wheat treatment and reseeded treatment, respectively (Table 6).

Table 6: N application rate, yield, N content and N uptake.

Treatment	N application rate (kg N ha^{-1})	Yield (kg DM ha^{-1})	N Content (g N kg DM^{-1})	N uptake (kg ha^{-1})
Reference	170	4368	19	82
Wheat	50	8211	15	118
Reseeded	50	6808	18	120

3.1.3 Soil temperature

Figure 14 presents the soil temperature of all three treatments and air temperature. The soil moisture gradually increased from approximately 10°C in the beginning in May to an average of 20 °C during June until August. From August onwards the temperature gradually decreased again. The air temperature followed the same pattern, but was generally lower than the soil temperature.

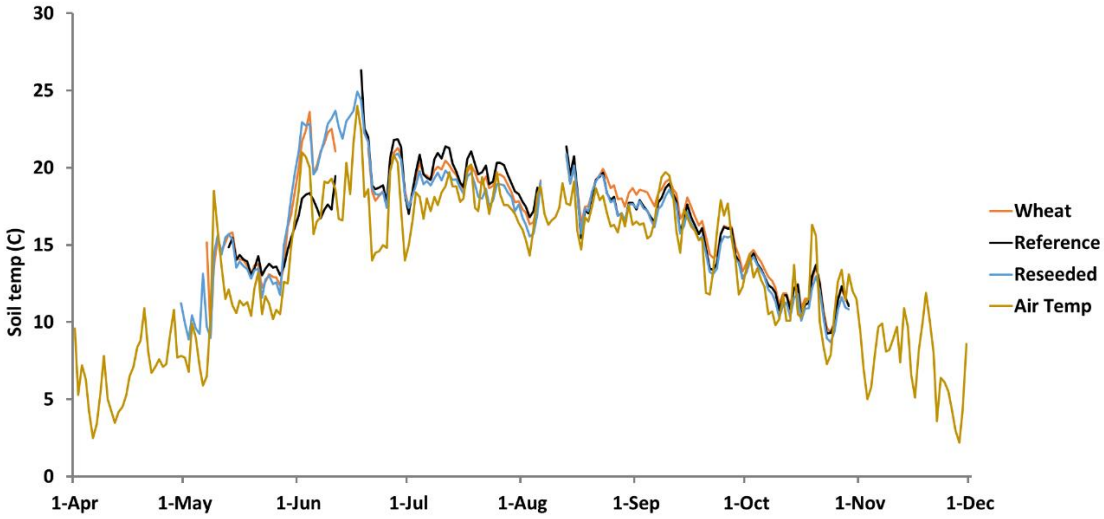

Figure 14: Soil temperature for all three treatments and air temperature.

3.1.4 Soil moisture

Figure 15 presents the soil moisture of all three treatments and precipitation. In general, the soil moisture increased with time for all three treatments from 5-15% in May to 25-40%. June and especially September were dry periods, whereas May was relatively wet.

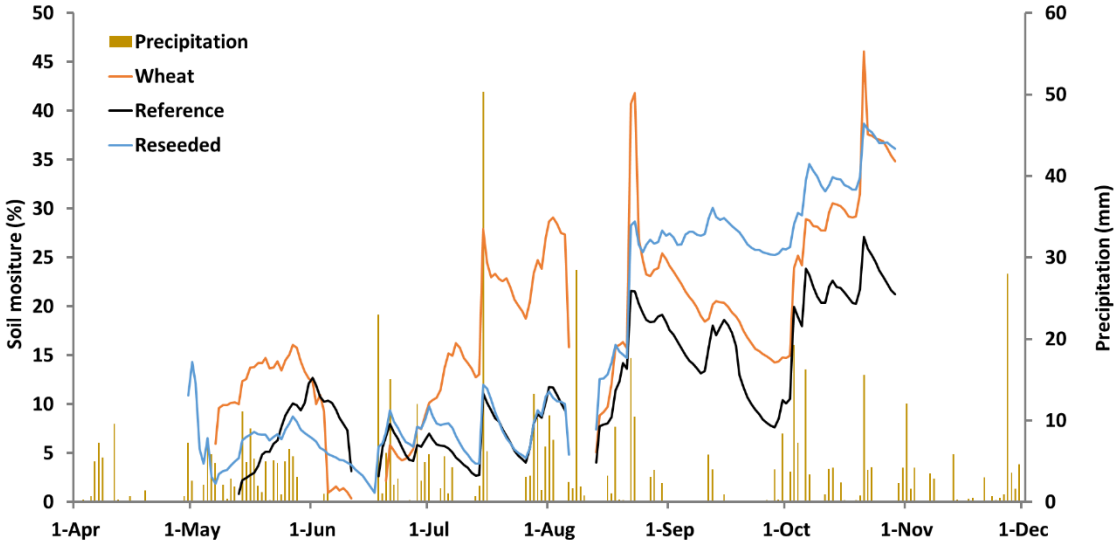

Figure 15: Soil moisture content and precipitation

3.2 Gaseous emissions

3.2.1 Chamber method

Figure 16 shows the average N_2O-N flux of the three treatments throughout the whole experimental period. Fluxes ranges from 0 to 0.67 mg N_2O-N m^{-2} h^{-1} throughout the whole experimental period. Peak fluxes are mostly observed after events of manure application or tillage (in the figure indicated as vertical spotted blue lines). Firstly, fluxes are observed at the first two weeks of May for all three treatments due to tillage (reseeded and wheat treatments) and manure application (reference treatment). The second peak occurred in mid-June, directly after manure application. Small peaks of N_2O- emission were observed for both reference and reseeded. However, the highest flux were found for the wheat treatment. On the 7th and 14th of June, the wheat field was harrowed for mechanical weed control. The third, and also highest peak, occurred in middle of August, after harvest (wheat treatment) and manure application (reference and reseeded treatment). The fluxes dropped in September and from half September and onwards there were no fluxes observed.

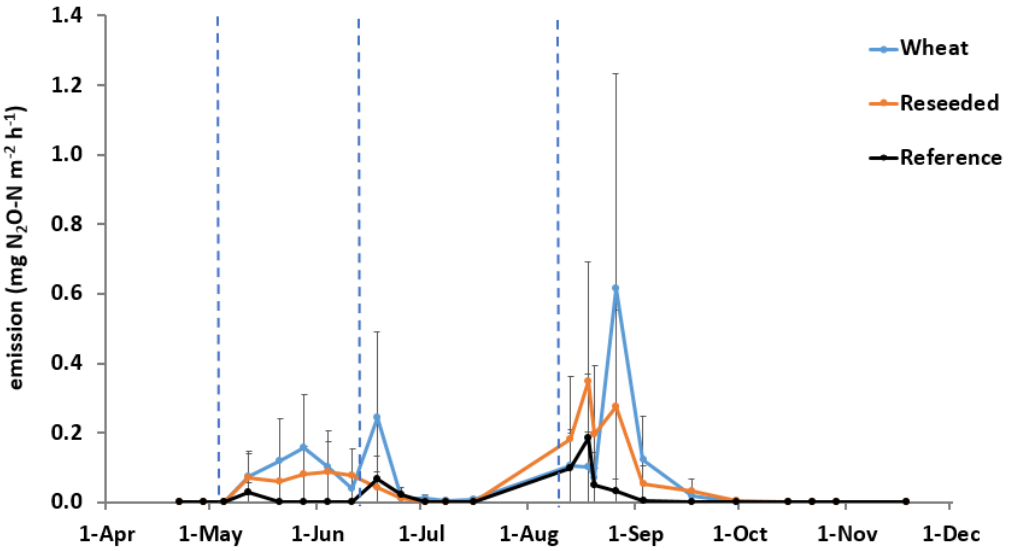

Figure 16: Average N_2O flux over time with the chamber method. The blue dotted lines indicate events of agricultural management: tillage, fertilization, harvest and sowing (n = 9).

3.2.2 Fast-box method

Fluxes from the fast-box ranged from 0 to 0.21 mg N_2O-N m^{-2} h^{-1} throughout the whole experimental period (Figure 17). Similar to the me chamber method, Peak fluxes are mostly observed after events of manure application or tillage (in the figure indicated as vertical spotted blue lines). fluxes are observed at the first two weeks of May for reseeded and the reference treatment due to tillage. Manure application in the beginning may did, however, not lead to any emission on the reference treatment. The second peak occurred directly after manure application in mid-June in which small peaks of N_2O- emission were observed for both reference and reseeded. Furthermore, high fluxes were found for the wheat treatment during this period due to mechanical weed control that was performed on the 7th and 14th of June. The third, and also highest peak, occurred in middle of August, after harvest (wheat treatment) and manure application (reference and reseeded treatment). The fluxes dropped in September and from half September and onwards there were no fluxes observed.

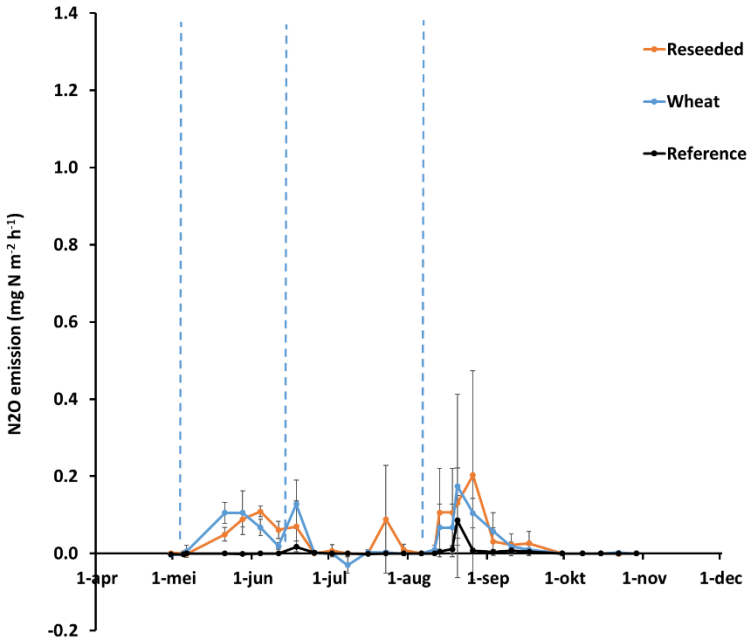

Figure 17: Average N_2O flux over time with the fast-box method. The blue dotted lines indicate events of agricultural management: tillage, fertilization, harvest and sowing (n = 6).

3.2.3 Eddy Covariance

3.2.3.1 Concentrations and basic fluxes from Eddy Covariance measurements

In Figure 18, half-hourly concentrations are visualized as box-whisker-plots separated into 15 days periods.

Concentration of CO_2 did not exhibit substantial changes during the six month campaign apart for the reference field from 1st July to 15th July, caused by pressure problems and valve issues. Medians were between 403 and 436 ppm considering their minimum and maximum. In addition, length of their IQRs is similar for all periods ranging between 20.1 and 73.7 ppm. In case of N_2O, values were between 2.3 and 46.6 ppb. N_2O concentration medians ranged between 313 and 326 ppb. In addition, median concentration of N_2O seemed to increase at all field during the campaign. This was caused by the exchange of the N_2 cylinder, used for autobackground corrections. The new cylinder was from another supplier, resulting in a change of the background concentration for N_2O. A remarkable influence of fertilization on measured concentrations was not found except for the reseeded Field in August. Considering the whiskers, values up to 360 ppb were reached. Generally, concentration of both gases was similar on all three fields. Average concentrations and their standard deviations are given in Table 7. An overview about the contribution of emission and deposition fluxes is given in Table 7 as well.

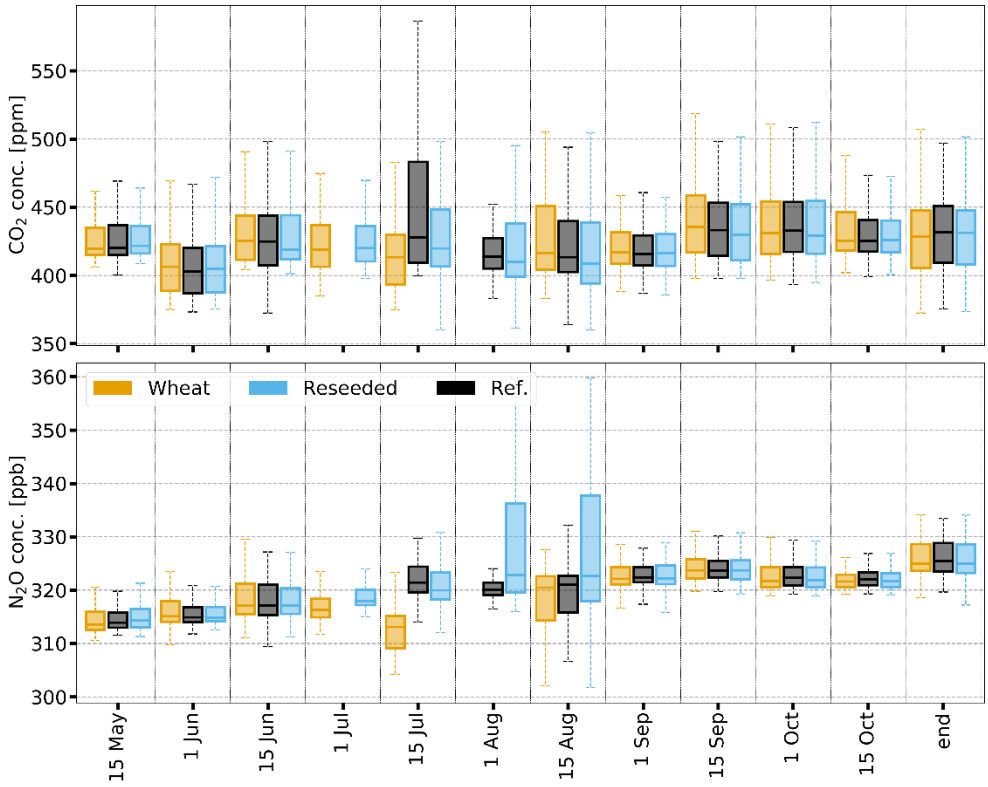

Figure 18 Time series of half-hourly CO_2 and N_2O concentrations represented as box-whisker-plots (box frame = 25% to 75% interquartile ranges (IQR), bold line = median, whisker = 1.5*IQR) and separated into 15 days periods in ppm and ppb, respectively.

Table 7: Mean (avg) and standard deviation (std) of concentrations (conc) and fluxes for CO_2 and N_2O. In case of half-hourly fluxes, the contribution of emission and deposition fluxes of CO_2 and N_2O for each field. Values refer to the entire campaign.

	CO_2 [flux unit: mg C m^{-2} h^{-1}; conc. unit: ppm]			N_2O [flux unit: µg N m^{-2} h^{-1}; conc. unit: ppb]		
	Wheat Field	Reseeded Field	Reference Field	Wheat Field	Reseeded Field	Reference Field
Emission [%]	55.0	50.0	44.0	73.0	76.0	68.0
Deposition [%]	45.0	50.0	56.0	27.0	24.0	32.0
Avg. Flux	-27.7	-76.3	-106.0	40.3	39.2	20.9
Std. Flux	300.0	321.0	309.0	99.7	88.6	71.3
Avg. conc.	431	429	431	320	322	320
Std. conc.	36.7	37.6	36.2	6.1	7.4	6.0
Data availability[%]	14.0	15.0	12.0	14.0	15.0	12.0

Due to fertilization and agricultural management, more emission fluxes were observed on the wheat and grass field. Generally, emission fluxes were low. Up to 5% of the emission fluxes of the wheat field were higher than 360 mg C m^{-2} h^{-1}; only 4% of the grass and 3% of the reference field. CO_2 deposition fluxes occurred more frequently on the reference field. CO_2

fluxes are comparable fluxes for example reported by Bajgain et al. (2018), Cardenas et al. (2022), Schmidt et al. (2012) for wheat and grass pastures.

For N_2O, emission fluxes prevailed on all fields (ca. 72 % on average). However, most emission fluxes were lower than 72 µg N m^{-2} h^{-1} leading to generally low N_2O emissions apart from fertilizing periods (see Figure 19).

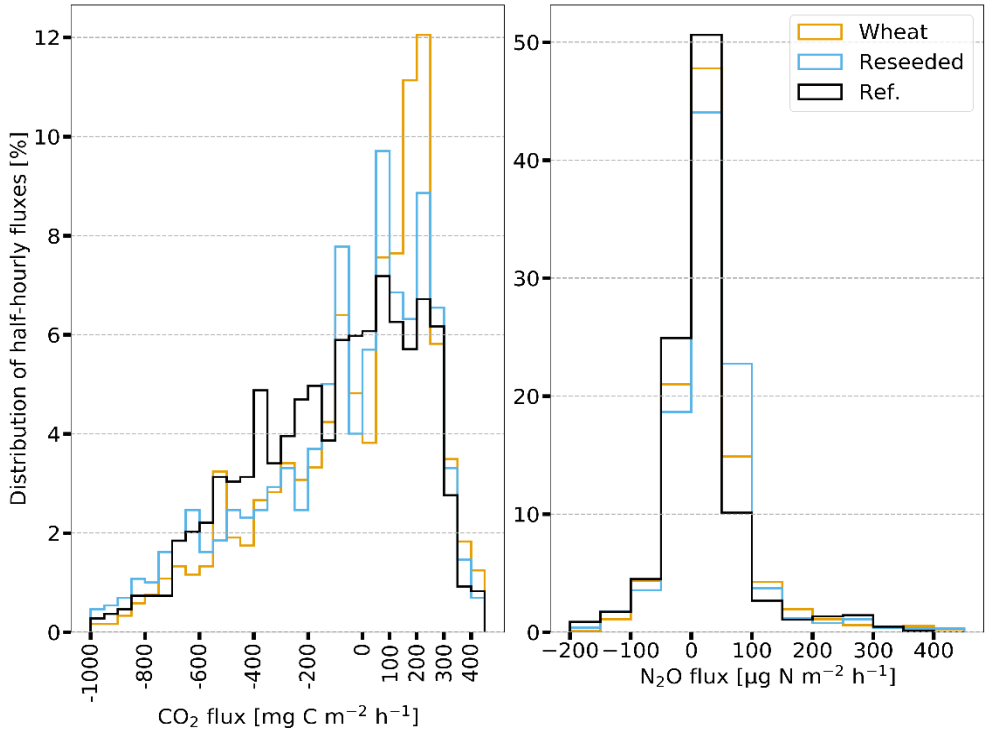

Figure 19: Histogram of half-hourly CO_2 (left) and N_2O (right) fluxes for wheat (orange), reseeded (blue), and reference field (black) during the entire campaign. CO_2 fluxes in mg C m^{-2} h^{-1}, N_2O fluxes are given in µg N m^{-2} h^{-1}.

A time series of CO_2 and N_2O fluxes is shown in Figure 20. At the wheat and reseeded field, emissions occurred until June and in the first weeks of August even at the reference field. This was related to the application of manure (see Table 1). Apart from those periods, deposition fluxes prevailed in the CO_2 flux time series of the different fields but with differences in their uptake potential considering the average flux (Table 7). On average, strongest carbon uptake was measured for the reference field as represented the flux medians, whereas the lowest uptake was found for the wheat field. Considering the last two month, flux pattern at all fields was in close agreement as seen by their diurnal patterns (Figure 21) since from mid of August agricultural management was practically the same for all fields due to the same vegetation. Generally, the diurnal pattern of CO_2 was nearly identical for all fields – deposition during the day and emission during the night. No diurnal cycles of CO_2 were made for June and July. Due to low data coverage during those months and the higher diurnal flux variability of CO_2 than N_2O apart from fertilization events, flux averages of CO_2 are biased.

For N_2O, the average fluxes of all fields were similar with slightly higher emission fluxes at the wheat and grass field. However, fluxes showed hardly any variability and were close to zero during the whole day (Figure 21) apart from mid to end of May and August, respectively. Emission fluxes up to 288 µg N m^{-2} h^{-1} were measured at the wheat field as example (Figure 20). This coincides with the application of manure.

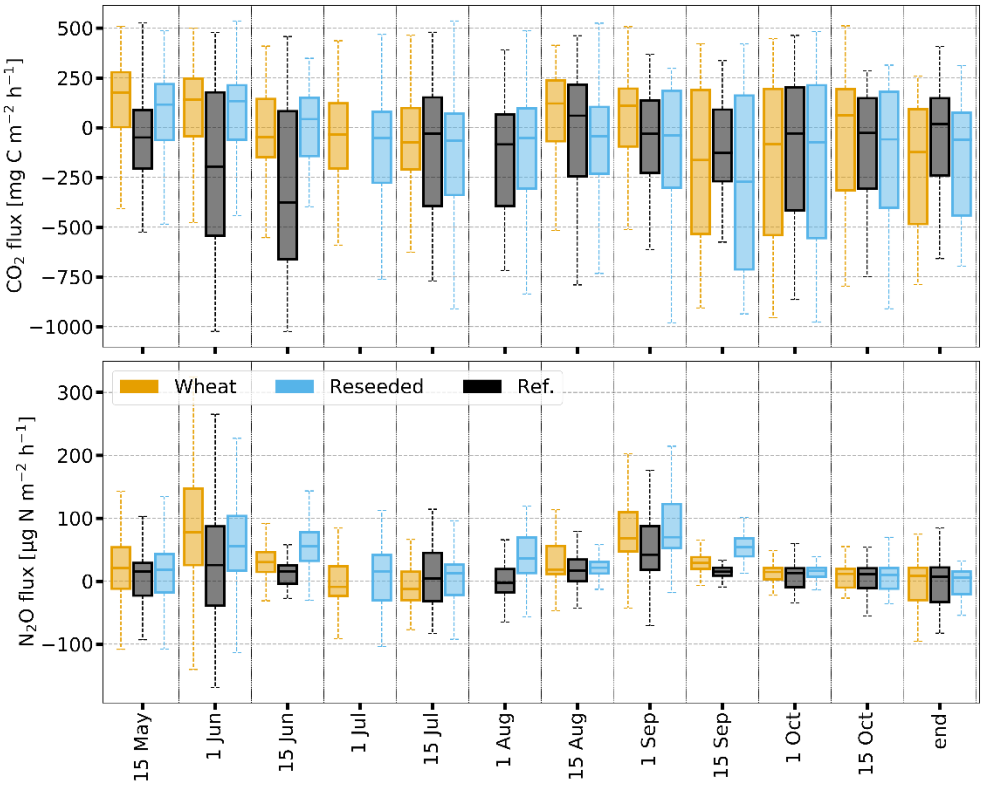

Figure 20: Time series of half-hourly CO_2 and N_2O fluxes represented as box-whisker-plots (box frame = 25% to 75% interquartile ranges (IQR), bold line = median, whisker = 1.5*IQR) and separated into 15 days periods in mg C m^{-2} h^{-1} and µg N m^{-2} h^{-1}.

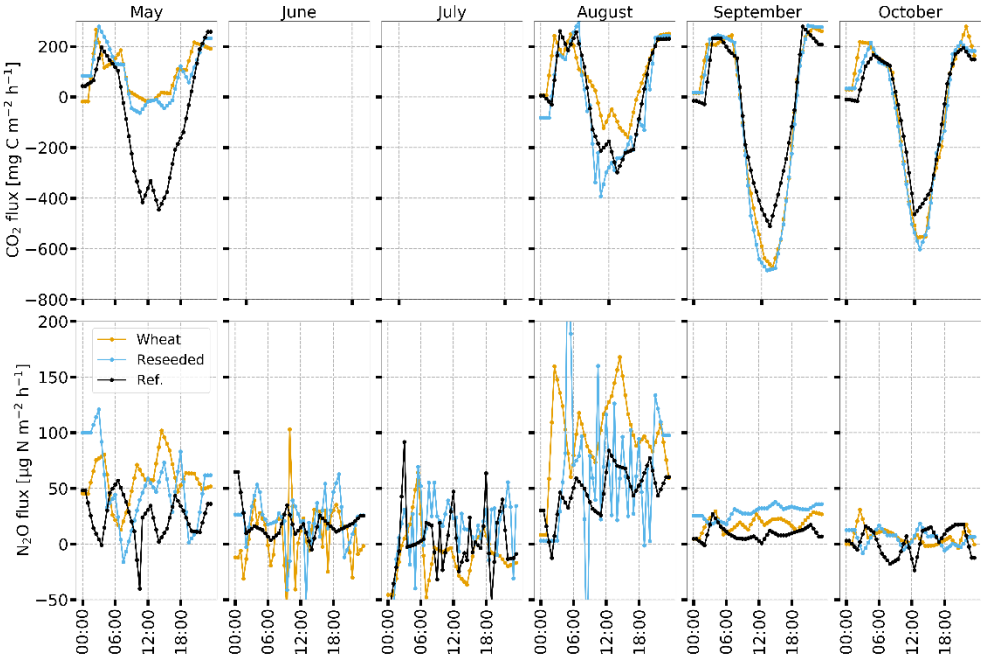

Figure 21: Averaged diurnal cycles of CO_2 (upper row) and N_2O (lower row) from May to October in mg C m^{-2} h^{-1} and µg N m^{-2} h^{-1}. Colours indicate different fields. Gaps in diurnal patterns were linearly interpolated.

3.2.3.2 Corrections for inlet long lines – damping

In the following, the results of the damping analysis done for each field are discussed. The corresponding Figure 22 to Figure 24 show the median damping factors of CO_2, H_2O, and N_2O depicted as box-whisker-plots.

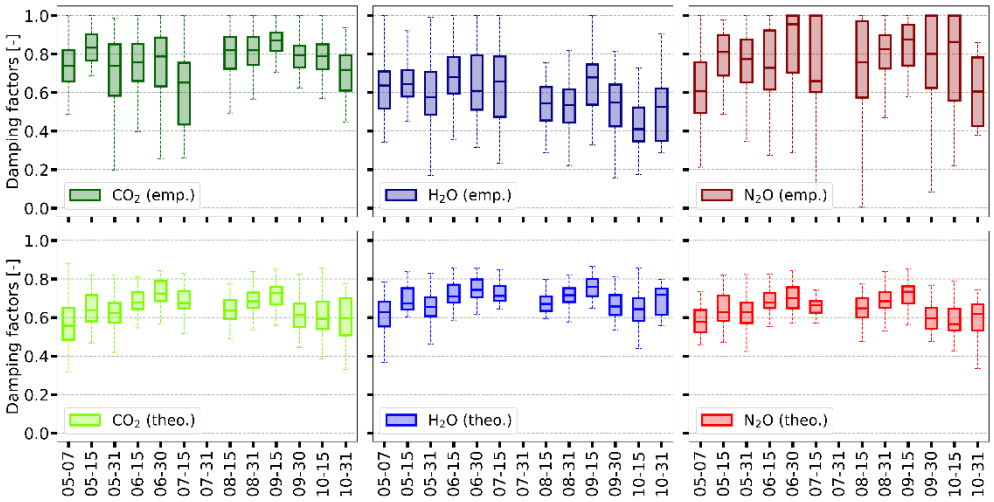

Figure 22: Damping factors of CO_2, H_2O, and N_2O for the wheat field represented as (bi)weekly box-whisker-plots (box frame= 25 % to 75 %/ interquartile range (IQR), bold line = median, whisker = 1.5*IQR). In the upper row, results of the empirical method (ICO) are shown, in the lower panel the results of the theoretical approach by Moncrieff et al. (1997).

For the wheat field, median damping factors of CO_2, H_2O, and N_2O were 0.79, 0.58, and 0.79 respectively, whereas the theoretical factors were 0.65, 0.69, and 0.65, respectively (Figure 22). In case of CO_2, (bi)weekly theoretical median damping factors were generally larger by ca. 0.13 on average. From both approaches, no obvious trend in damping values have been found. For H_2O, theoretical and empirical values were close to each other until mid of July. Afterwards, (bi)weekly median values of the empirical method were larger than their theoretical entity by ca. 0.15. For N_2O, the biweekly medians and their temporal pattern were similar to the values of CO_2, but N_2O damping factors had the largest variability.

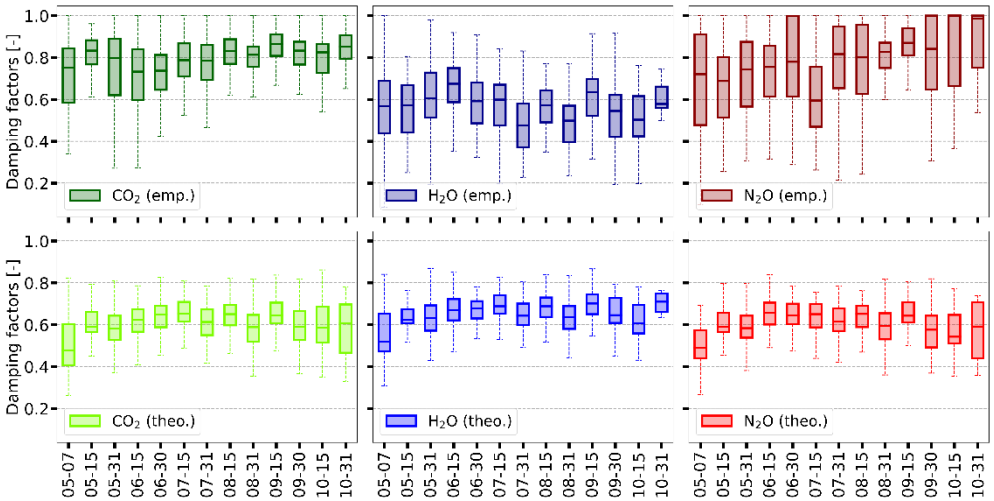

Figure 23: Analogue to Figure 22 but for the reseeded field.

Similar campaign wise medians were determined for the grass field (Figure 23). In Table 8, a summary of all campaign wise medians and their interquartile ranges is given. In Figure 24, the comparison is shown for the reference field.

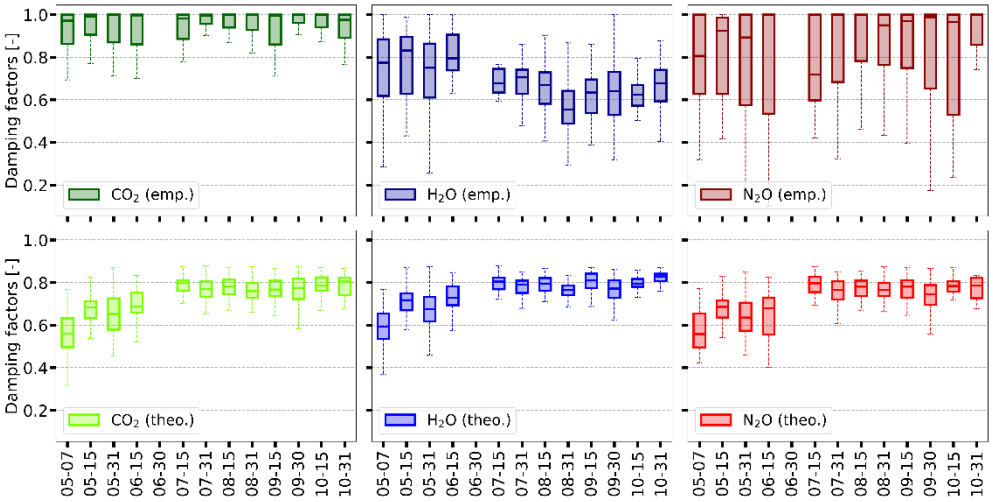

Figure 24: Analogue to Figure 22 but for the reference field.

In case of the theoretical damping, it is assumed that flux attenuation gets lower for shorter sample lines. The reduction from 90 m to 13 m should theoretically lead to a decrease in flux damping of ca. 0.13. However, this could not be verified by the measurements. An increase in the flux damping of 0.14 was found for the H_2O flux. The tube shortening had no effect on the CO_2 flux. The CO_2 flux damping is even negligible. Surprisingly, flux damping was substantially larger for the shorter sample line in case of H_2O. For N_2O, a campaign wise median close to CO_2 was obtained. However, N_2O flux damping values exhibited a large variability resulting in a large uncertainty of the corrected fluxes if their median damping factors would have been chosen.

Table 8: Campaign wise damping medians and their lower (25 %) and upper (75 %) percentiles of CO_2, H_2O, and N_2O calculated with the empirical (ICO) and theoretical method (THEO) for each field.

Field		Median			Low Quar.			Upper Quar.		
		CO_2	H_2O	N_2O	CO_2	H_2O	N2O	CO_2	H_2O	N_2O
Wheat	ICO	0.79	0.58	0.79	0.69	0.46	0.65	0.87	0.70	0.93
	THEO	0.65	0.69	0.65	0.58	0.64	0.59	0.72	0.75	0.72
Reseeded	ICO	0.80	0.57	0.80	0.70	0.44	0.64	0.88	0.67	0.94
	THEO	0.61	0.66	0.62	0.53	0.59	0.54	0.68	0.71	0.68
Ref	ICO	1.0/ 1.0	0.77 /0.63	0.90 /0.98	0.86 /0.93	0.63/ 0.55	0.59/ 0.68	1.0/ 1.0	0.89/ 0.72	1.0/ 1.0
	THEO	0.64/ 0.78	0.67/ 0.79	0.65/ 0.77	0.55/ 0.74	0.59/ 0.75	0.56/ 0.73	0.71/ 0.82	0.74/ 0.82	0.71/ 0.81

At all three fields, half-hourly damping factors of N_2O exhibited a large variability. In addition, half-hourly N_2O fluxes were very low and the magnitude of the diurnal pattern was not larger than ±36 µg N m^{-2} h^{-1}. Probably, most N_2O fluxes were close to the detection limit of the instrument making a campaign-wise determination of a flux damping challenging. As a

solution, we suggest to correct N_2O fluxes with damping factors of CO_2 since both gases are likely inert.

The difference in H_2O damping of the wheat and grass field regarding the first and second half of the campaign may be related in a certain degree to tube degradation. The sample lines were very long and a contamination with pollens, dust, or other minerals over time could not be fully prohibited even if a proper filter mesh protects the inlet.

In case of H_2O, an increase in the flux damping while reducing the length of the sample line is unusual and contradicts theoretical assumptions. It had even any impact on the flux damping of CO_2. Both observations are difficult to explain. If the tube was twisted to certain degree after cutting, water droplets or other particles could have been accumulated in certain parts of the tube resulting in a larger damping of H_2O. Due to the shorter inlet line, the sonic of the reference field was closer to the field border. Thus, contribution of wheat and grass field to the reference fluxes were definitely larger after the shift in position.

In conclusion, the comparison of the two flux damping approaches showed that the theoretical flux damping approach, a standardized method for calculating flux damping, is not suitable for the measurement setup. Predicted flux damping values of CO_2 and N_2O are rather large and contradictions regarding the tube line effect were found. Since different vegetation types each of them with an individual surface roughness are included in the flux foot print, a theoretical turbulence spectrum may not be the appropriate choice for the setup.

3.2.4 Cumulative fluxes and comparison of the three methods

3.2.4.1 Static chamber method

Cumulative fluxes increased over time right after the manure application, tillage and harrowing events in the beginning of May, beginning and mid of June and the beginning of August (Figure 25). The cumulative emission was highest for wheat (3.36 kg N_2O-N ha^{-1} ± 1.43), followed by reseeded (2.67 kg N_2O-N ha^{-1} ± 1.25) and lowest for the reference treatment (0.86 kg N_2O-N ha^{-1} ± 1.06). One-Way ANOVA analysis and post-hoc test Tukey show that the cumulative emission of both wheat ($p < 0.01$) and reseeded ($p= 0.02$) are higher than reference. No significant difference was found between wheat and reseeded.

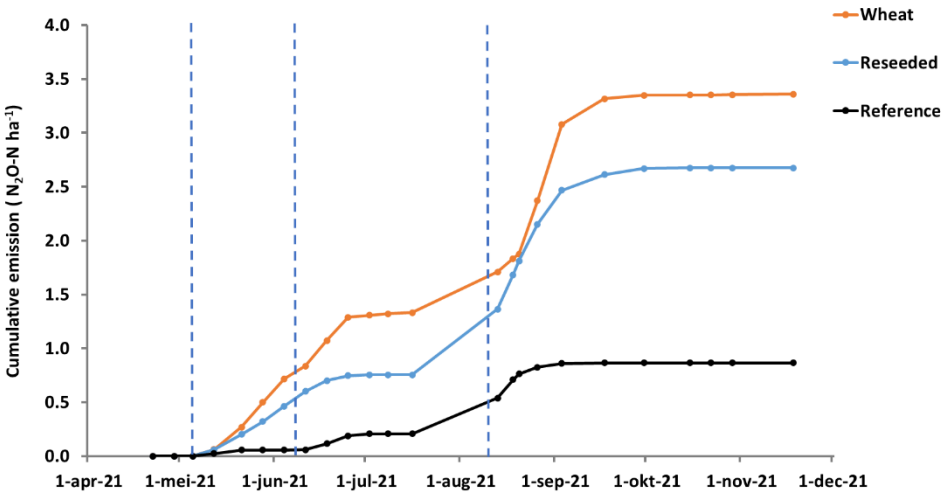

Figure 25: Average cumulative flux for the static chamber method. The blue dotted lines are agricultural events: fertilization, tillage and sowing (n=9).

3.2.4.2 Fast-box method

Similar to the static chamber measurements, the cumulative fluxes of the fast-box method increased over time after the manure application, tillage and harrowing events (Figure 26). Cumulative ranges from 1.41 kg N_2O-N ha^{-1} for wheat, 1.66 kg N_2O-N ha^{-1} for reseeded to 0.17 kg N_2O-N ha^{-1} for the reference treatment. One-Way ANOVA analysis and post-hoc test Tukey show that the cumulative emission of both wheat ($p < 0.01$) and reseeded ($p = 0.02$) are higher than reference. No significant difference was found between wheat and reseeded.

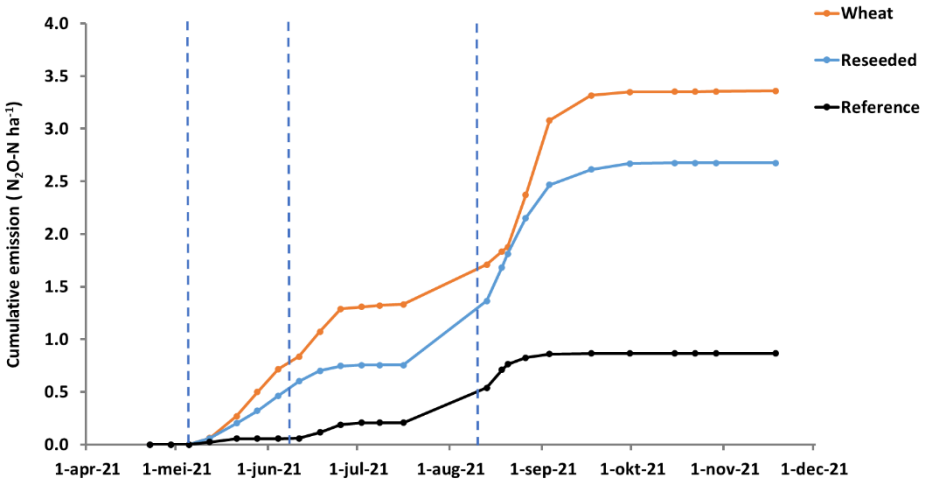

Figure 26: Cumulative N_2O exchange in kg N ha^{-1} estimated from fast-box measurements.

3.2.4.3 Eddy Covariance

Before the comparison of the Eddy Covariance measurements to chamber measurements is taking place, the results of the area weighting approach are shown for CO_2 and N_2O in Figure 27 and Figure 28, respectively. The area weighting approach did not affect the carbon deposition of the refence field significantly. Both approaches – the area weighting and the original – predicted more or less the same deposition at the end of the campaign. Following the area weighting approach, the wheat field tend to be an emission source for carbon, whereas the grass field tend to be a weak carbon sink. Using the original approach, the grass field appeared to be a slightly stronger carbon sink compared to the weighted approach, and the wheat field likely lost carbon during the measurement period. In conclusion, the wheat field was more likely a carbon source, the reseeded field appeared to be a weak carbon sink, and the reference field stored carbon during the measurement period. The changes in the direction of the cumulative curves were related to agricultural management: Right after start of the campaign, emission prevailed due to fertilization and tillage. As plant growth started, CO_2 was taken up by plants until harvesting/mowing leading to an emission phase. In the last two months, carbon was taken up again. The increase in CO_2 fluxes of the aera weighting approach close to the end of the campaign is caused by the uptake occurred at the reference and the reseeded field.

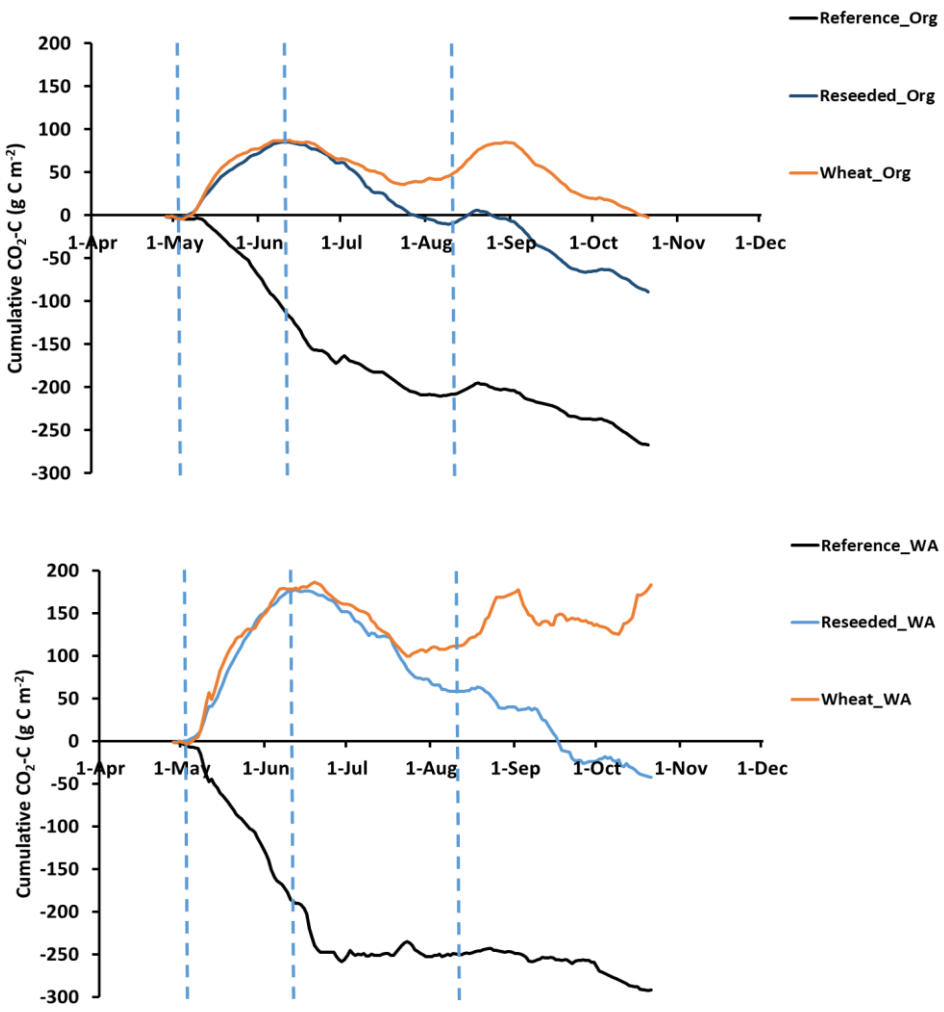

Figure 27: Cumulative CO_2 exchange of all fields differentiated by colours in g C m^{-2}. The upper figure represents cumulative curves using directly calculated fluxes without area weighting considering the total footprint indicated by 'Org'. The bottom figure represents cumulative curves using the area weighting approach and named as 'WA'. Gap-filling of CO_2 fluxes was done following the MDS approach by Wutzler et al. (2018).

Compared to CO_2, N_2O exchange was about three orders of magnitude smaller. As expected, N_2O emissions were larger at the wheat and reference field probably due to extensive agricultural management. Increases in N_2O fluxes were found within periods affected by fertilizer application and mowing/harvesting like in May and August. Apart from these periods, N_2O exchange was close to zero or only slight emissions were observed.

At last, a comparison to flux chamber measurements was made for N_2O. Both - EC and fast-box chamber measurements - showed lowest emission for the reference field, and the other fields exhibited similar emission estimates. For the latter, flux chamber measurement resulted in lower emissions by factors of approx. 2.5 and 2.8 to EC for the wheat and reseeded considering unweighted fluxes, respectively. Largest differences were found for the reference field (Figures 27 and S1). With flux chamber measurements, capturing the flux variability of the reference field was not possible. Best agreement was achieved for the wheat field. For the

reseeded field, the peak in flux chamber measurements during mid of May could not be verified by EC measurements. Probably, emissions at that field were close to or below the detection limit of the QCL. In case of N_2O, flux detection limit (Langford et al., 2015) was at 37.8 µg N m^{-2} h^{-1}, which is close to the average flux.

Apart from the differences in flux amplitude, the temporal flux pattern agreed well. The duration of emission phases covering May to June and August was captured by both measurement techniques. As written before, disagreements outside the management periods are probably related to the generally low N_2O background exchange, which was below the flux detection limit of chamber measurement approach. All results are summarized in Table 9.

Uncertainties of these flux budgets are difficult to quantify. For CO_2, total random error calculates from the random uncertainty due to gap-filling, which is defined as standard deviation of fluxes used for gap-filling, and the random flux error given by Finkelstein and Sims (2001) assuming that errors are independent from each other:

$$\delta_{\text{total}} = \sqrt{\sum_{i=0}^{n}\left(\varepsilon_{\text{rand err,i}}\right)^2 + \sum_{i=0}^{n}\left(\varepsilon_{\text{gap-filling,i}}\right)^2} \quad (4)$$

Systematic uncertainties are not accounted. These are related to the instruments and their arrangement of the instrument, the footprint, flux processing options, and advection fluxes. Considering the original approach, CO_2 total random uncertainties were between 10 and 12 g C m^{-2} depending on the field. The application gap-filling algorithm following Wutzler et al. (2018) seemed to be reasonable since variability in flux pattern of CO_2 can be modelled well. If all values were considered as gaps, carbon estimates differed only by 3 g C m^{-2} from the original values.

From the random forest approach (RF), soil water volume, soil temperature, and concentration were found to be most important for the gap-filling of N_2O fluxes. On average, 26%, 16%, and 24% of the flux dynamics could be explained by soil water volume, concentration, and soil temperature, respectively. The RF approach showed a better performance than statistical gap-filling approaches like a combination of the mean diurnal variation (MDV) principle (Falge et al., 2001), which assumes a certain similarity in diurnal pattern of ±3 days, whereas remaining long-term gaps were replaced by monthly averages of the specific half-hourly value. This approach resulted in lower emissions estimates considering the unweighted fluxes and unusual deposition fluxes occurring in July, in particular at the wheat field. We didn't notice any issues with instrument performance. During the same time, emission prevailed at the reseeded field and exchange was close to zero at the reference field. At the wheat field, canopy was growing substantially during that month (Table 5). Supposedly, canopy height was close to measurement height leading to uncertainties measurements of field turbulence. Thus, calculated nitrogen budgets during that time should be taken with care. Due to the large flux variability of N_2O, it is questionable if the applied statistical gap-filling approaches are able to reproduce the flux pattern, in particular the use of monthly averages, which may underestimate the flux since short-term emissions were not captured. In addition, measurements were taken at specific times of the day leading to biased averages.

For the installed EC setup, the footprint is the major uncertainty. With the area weighting approach, we tried to evaluate the influence of the footprint on carbon and nitrogen budgets.

For our purposes, the area weighted fluxes may be interpreted as upper/lower flux indicators showing at least the tendency of the exchange for each field. Similar to CO_2, emission of N_2O was observed at the end of the measurement campaign, which was related to the application of the area weighting approach. The latter is also responsible for deposition fluxes of N_2O, which were not verified by the measurements. From these findings, we conclude that the wheat field lost carbon during the campaign, whereas storage of carbon happened at the reference field and to a certain extend at the reseeded field. Nitrogen was released on all fields with largest emissions occurring at the wheat and reseeded field.

Overall, N_2O background fluxes are similar to recent studies by Cowan et al. (2016,2020), Liang et al. (2018), Lognoul et al. (2019) and Murphy et al. (2022) for example being mostly lower than 1 nmol m^{-2} s^{-1}. During agricultural management like ploughing and fertilizing, highest emission fluxes were recorded. Fluxes were in the same order of magnitude but depends strongly on soil type, crop type, amount of in/organic fertilizer application, and micrometeorology.

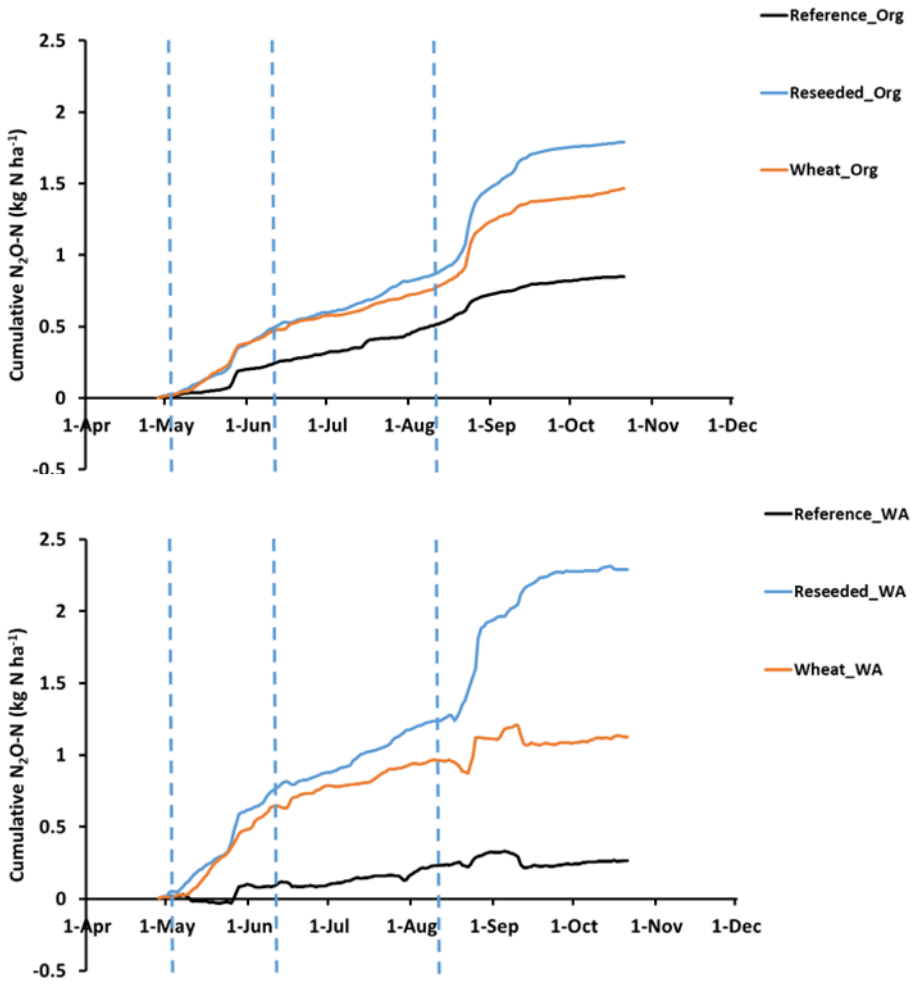

Figure 28: Cumulative N_2O exchange of all fields differentiated by colours in kg N ha^{-1}. The upper figure represents cumulative curves using directly calculated fluxes without area weighting considering the total footprint indicated by 'Org'. The bottom figure represents cumulative curves using the area weighting approach and named as 'WA'. Gap-filling of N_2O fluxes was done by using the RF approach.

Since substantial data gaps were in the N_2O flux time series, emission factors obtained from gap-filled time series should be taken with care. Considering the entire time series, 50 Kg N ha^{-1} were applied on the wheat and grass field leading to emission factors between 2.2 and 4.6%. On the reference field, 170 kg N ha^{-1} were applied in total, which results in EFs from 0.2 to 0.5%. Values for the reference site are likely comparable to EF reported for perennial grasslands (see Table 3 of Lognoul et al. (2019).
Table 9 presents the cumulative CO_2 and N_2O flux estimated from Eddy Covariance (original and area weighted) and flux chamber measurements for all fields in their respective units.

Table 9: Cumulative CO_2 and N_2O flux estimated from Eddy Covariance – original (org) and area weighted (aw) - and fast-box flux chamber measurements for all fields in their respective units.

	Eddy Covariance			
	CO_2 [g C m^{-2}]		N_2O [kg N ha^{-1}]	
	Org	Aw	Org	Aw
Wheat	3.3	184	1.5	1.1
Reseeded	-90	-44	1.8	2.3
Reference	-268	-292	0.8	0.3

When we convert these data into CO_2 equivalent emissions (using GWP 273 for N_2O, https://www.epa.gov/ghgemissions/understanding-global-warming-potentials, last access: 27 June 2022), Table 10 the net area flux data for both CO_2 and N_2O expressed in CO_2-eq. The total CO_2-eq emission is highest for the wheat treatment and lowest for reference. The table implies that the relatively contribution of N_2O is low, but part of the CO_2 emission is so called 'short cycle' – sequestered C in manure and then released by decomposition of the manure. Therefore, The CO_2 emission cannot be directly compared with the N_2O emission.

Table 10: Net area flux data CO_2 equivalent emission to the atmosphere.

Field	Area weighted net fluxes		
	g CO_2 m^{-2} eq		
	CO_2*	N_2O	Sum
Wheat	675	47	722
Reseeded	-161	99	-62
Reference	-1071	13	-1058

*The measured CO_2 is partly 'short-cycle' and should therefore not directly compared with the N_2O- emission.

3.2.4.4 Comparison of the methods

Table 11 presents the cumulative CO_2 and N_2O for all three methods. The static chamber method has the highest emission for all three treatments, with 3.36, 2.67 and 0.86 kg N_2O-N ha^{-1} for wheat, reseeded and reference, respectively. The cumulative emissions with the fast-box chamber method were much lower, with 1.41, 1.66 and 0.17 kg N_2O-N ha^{-1}. The cumulative emissions measured with the Eddy Covariance method (Aw; weighted area) are in between these emissions measured with the chambers for both reseeded (2.3 kg N_2O-N ha^{-1}) and reference (0.3 kg N_2O-N ha^{-1}). The cumulative emission for wheat (1.1 kg N_2O-N ha^{-1}) is lower for the Eddy Covariance method in comparison to the other two methods.

Table 11: Comparison of cumulative CO_2 and N_2O.

	Eddy Covariance				Fast-box chamber measurement	Picarro static chamber
	CO_2 [g C m^{-2}]		N_2O [kg N ha^{-1}]		N_2O [kg N ha^{-1}]	N_2O [kg N ha^{-1}]
	Org*	Aw**	Org*	Aw**	Fast-box method	Static chamber
Wheat	3.3	184	1.5	1.1	1.41	3.36
Reseeded	-90	-44	1.8	2.3	1.66	2.67
Reference	-268	-292	0.8	0.3	0.17	0.86

*Org (Original): Cumulative emission calculated by using directly calculated fluxes without area weighting considering the total footprint.

** Aw (Area weighted): cumulative emission calculated by using the area weighting approach.

The cumulative fluxes throughout the experimental period differs with the three methods (Figure 29). All three methods show increasing cumulative fluxes at the same time, but the magnitude differs (i.e. the slope for each methods). This can partly explain the difference in the total N_2O emission at the end of the experiment. Furthermore, the relatively high estimation of the Picarro method can also be partly explained by a measurement gap for one month, between mid-July and mid-August. Due to the lineair interpolation for the Picarro method, the cumulative N_2O emission increased substantially whereas the cumulative N_2O emission for the eddy-covariance and fast-box method does not.

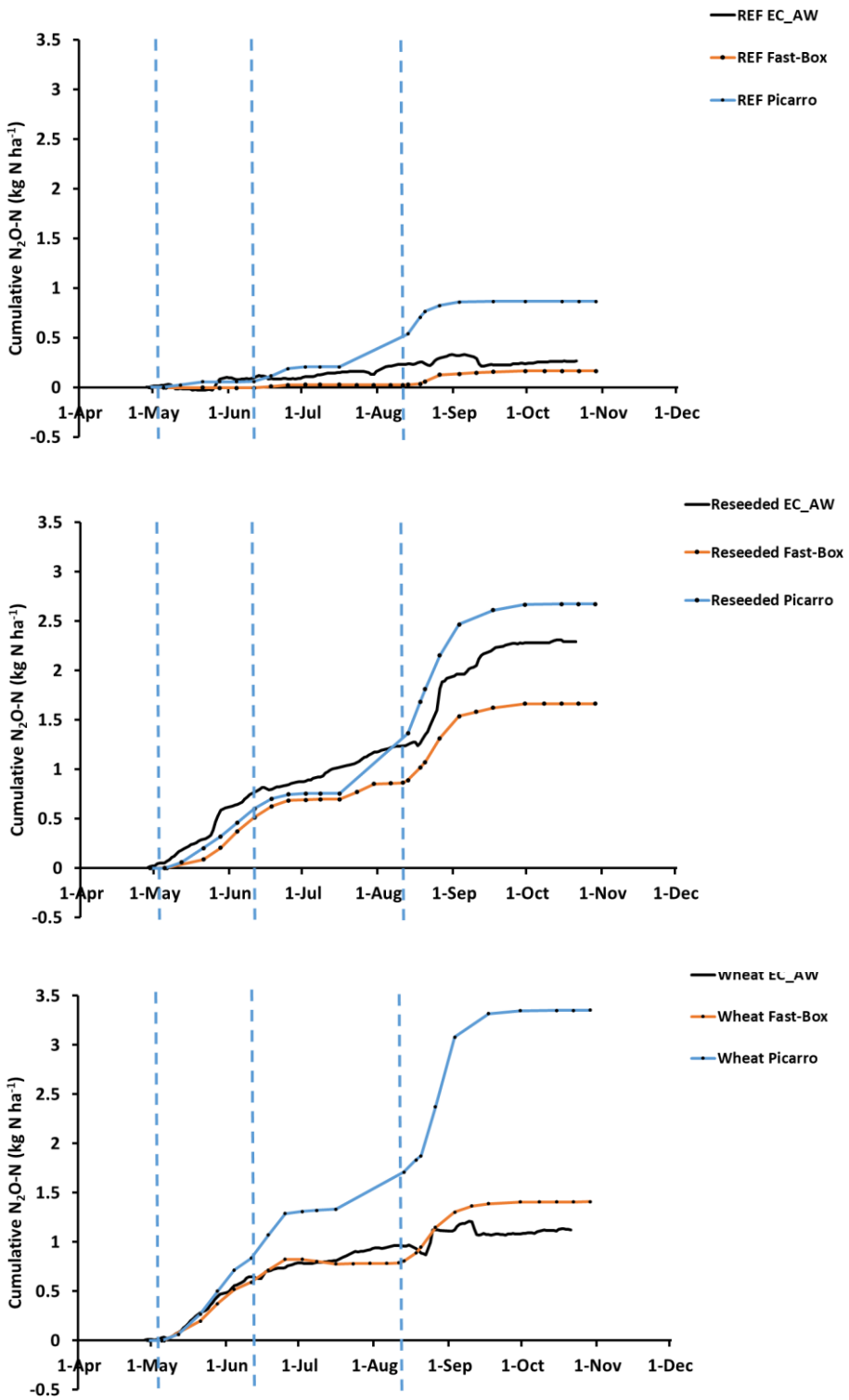

Figure 29: Comparison of the cumulative N_2O exchange of all fields for all methods. For this comparison, the weighted area approach is used for the Eddy-Covariance method

Table 12 shows relatively large differences of the cumulative emission between fast-box and the Picarro static chamber method. During the measurement campaign, the aim was to measure on the same day, but this was not always the case due to practical reasons. This could have led to different fluxes when the measurement were not performed on the same day. Therefore, Table 12 shows the cumulative emissions once more for only the fluxes that were measured on the same day. To do so, the measurement of the 30th of April, 5th and 6th of May and 23th of July had to be removed. This leads to a smaller difference of the cumulative emission between both methods.

Table 12: Comparison of cumulative CO_2 and N_2O with flux measurements on the same day only.

	Fast-box chamber measurement	Picarro static chamber
	N_2O [kg N ha^{-1}]	N_2O [kg N ha^{-1}]
	Fast-box method	Static chamber
Wheat	1.41	2.88
Reseeded	2.27	2.88
Reference	0.20	0.49

Nevertheless, the difference in cumulative N_2O- emission is mostly explained by differences in N_2O fluxes. Supporting Figure S3 shows an example of flux data of individual fast-box and static chamber measurement on the exact same location on each treatment. Highest fluxes were observed during August, in which the Picarro chamber method estimated consistently a higher flux than the fast-box method. That has resulted in a higher cumulative emission for the Picarro chamber method. On the contrary, low fluxes were estimated somewhat similar for both methods.

3.3 Interpretation of the results

3.3.1 Effect of grassland renewal on gaseous emissions

In terms of carbon, results of the Eddy Covariance method shows that the wheat field, when corrected with the weighted area approach, lost carbon during the measurement period. The effect of tillage causes a loss of carbon through CO_2 in the first weeks for both the reseeded and the wheat treatment. As plant growth started at the wheat treatment, CO_2 was taken up by plants until harvesting leading to an emission phase. In the last two months, carbon was taken up again due to sowing of fodder radish. However, at the end of the measurement period there was still a major net CO_2 exchange of 184 g C m^{-2} (1.84 tonnes C ha^{-1}) to the atmosphere, making the wheat treatment likely a carbon source. This means that tillage and subsequently transforming grassland to arable land is likely to be a carbon source. For the reseeded treatment, tillage causes a high loss of C in the first weeks as well, but as the new grass started to grow, carbon was taken up.

The loss of C in the first weeks was already compensated in August and at the end of the measurement campaign the net C exchange was -44 g C m^{-2} (0.44 tonnes C ha^{-1}). The reseeded treatment therefore appeared to be a small C sink. Therefore, despite renewing the grass, the loss of C is relatively fast compensated within a few months and this concludes that

grassland renewal does not lead to C loss. The reference treatment took up C during the whole measurement period. At the end of the campaign, the reference field took up 292 g C m^{-2} (2.92 tonnes C ha^{-1}), making the reference treatment a relatively big C sink. In terms of carbon storage and climate mitigation, permanent grassland would be the preferred option over conversion to arable land and grassland renewal. In case of the latter, however, grassland renewal is considered to be important to maintain the yield and nutritional value of the grass, as well as to keep up other ecosystem services related to grass production, such as soil quality (Kayser et al., 2018). Luckily, the results of the experiment show that periodical grassland renewal does not lead to C loss on the longer term. Furthermore, the temporary C loss for the reseeded treatment was already compensated at the end of the measurement period, which was only a period of four months. Continuing the experiments for, for example one year, could result in net C uptake for this treatment.

In terms of nitrogen, the cumulative emissions throughout all three methods varied ranged from 1.1-3.36 kg N_2O ha^{-1} for wheat, 1.66-2.67 kg N_2O ha^{-1} for reseeded and 0.17-0.86 kg N_2O ha^{-1} for the reference treatment. The cumulative emissions variation among the methods are relatively high and somewhat contradictory. The cumulative emissions observed with the static chamber method were highest for all treatments, in which the wheat treatment had the highest emission of 3.36 kg N_2O ha^{-1} followed by reseeded (2.67 kg N_2O ha^{-1}) and reference (0.86 kg N_2O ha^{-1}).

On the other hand, the cumulative emissions observed with the fast-box method were lowest except for wheat. With this method, the highest emissions were measured for the reseeded treatment (1.66 kg N_2O ha^{-1}), followed by wheat (1.41 kg N_2O ha^{-1}). For the reference field almost no N_2O- emission was observed (0.17 kg N_2O ha^{-1}). The cumulative N_2O- emission for the Eddy Covariance method are in between the observed cumulative emissions with the chamber measurements except for wheat. The highest emission measured with the Eddy Covariance was observed for the reseeded field (2.3 kg N_2O ha^{-1}), followed by wheat (1.1 kg N_2O ha^{-1}) and reference (0.3 kg N_2O ha^{-1}).

It was hypothesized that N_2O- emissions after grassland renewal are enhanced in comparison to those of permanent grassland due to increased N mineralization. For all methods the reference treatment had the lowest cumulative emission (0.17 – 0.86 Kg N ha^{-1}). Similar studies with grassland renewal experiments report N_2O- emissions varying from 0.4-2.6 (Biegman et al., 2014; Cowan et al., 2016; Velthof et al., 2010) for the control (permanent grassland) treatment. The cumulative N_2O for the static chamber method are within the range of these studies, whereas the cumulative for the fast-box method and EC method is lower in the present study in comparison to the other studies. Emissions due to renewal are in general a bit higher and varies from 1.2-3.5 kg N ha^{-1} for grassland renewal (Biegman et al.,2014; Davies et al., 2001; Velthof et al., 2010; Buchen et al., 2017), which is in the same range as found in the present study for all methods. Furthermore, studies with grassland conversion to cropland report the highest N_2O- emission. These emissions varies from 1.5-8.2 kg ha^{-1} (Reinsch et al., 2018; Buchen et al., 2017; Helfrich et al., 2020).

The peak emissions (changes in direction of the cumulative curves) found in the present study are related to agricultural management. The peak emission events were right after the start of the campaign (fertilization and tillage), fertilization events on June 17 and August 12 and harrowing on the 7^{th} and 14^{th} of June. Tillage may temporarily increase the mineral N content due to (1) ploughing of stubbles and roots that resulting in net mineralization of N, (2) the absence of crop N uptake directly after ploughing, and (3) enhanced mineralization of soil organic nitrogen due to ploughing. This may all lead to higher direct or indirect (emissions after leaching of mineral N) emissions of N_2O (Velthof et al., 2010). However, the mineral N

content at the reseeded field did not increase after tillage, but slightly declined. On the other hand, the mineral N content did slightly increase after tillage for the wheat field in the weeks after tillage, but this this is a combination of tillage and fertilization. Furthermore, an increase of mineral N is more clear after fertilization, which is clearly visual on Figure 13. N_2O- fluxes corresponds with the increase of mineral N as shown in Figures 25, 26 and 28.

3.3.2 Method comparison

Even though there is a lot of variation between the methods, peak emissions (i.e. changes in the direction of the cumulative curves) were found at events related to agricultural management for all three methods, but the difference lies in the absolute fluxes that are measured. Cumulative N_2O emission varied from 1.1-3.6 kg N_2O ha^{-1} for wheat, 1.66-2.67 kg N_2O ha^{-1} for reseeded and 0.17-0.86 kg N_2O ha^{-1} for the reference treatment. There are four factors that possibly explains the difference of the cumulative emissions between all three methods, especially between the fast-box and chamber method. Firstly, there is a large difference in the temporal resolution between the Eddy Covariance, fast-box and chamber method, as the Eddy Covariance measures each field every 1.5 hour and the other two methods only weekly. On the one hand, peak emissions could have been missed in between two measurements which could lead to an underestimation of the cumulative emission. On the other hand, the cumulative emission of both chamber methods is calculated by using a linear interpolation between two measurements. In doing so, the assumption is made that the measured flux takes several days. This could lead to an overestimation of the cumulative flux. Second, there is a difference in the spatial resolution; the Eddy Covariance covers a much higher area (footprint) than the fast-box and chamber method. Third, we have tried to measure with the fast-box and chamber method on the same day, but this was not always possible due to logistics. This could have led to different measured fluxes, and as a consequence, differences in the calculation of the cumulative emission. Third, there is a measurement gap of four weeks for the chamber method between mid-July and mid- August due to practical reasons. Figure 25 shows a relatively large increase in the cumulative emission in this period due to high fluxes right before and after the gap. The fast-box method has, therefore, a bit more measurement points than the chamber method (28 vs 24 measurements). However, Table 12 shows a comparison of the cumulative emission of both methods when measurements were performed on the same day. This analysis shows a smaller difference of the cumulative emission of both methods. Nevertheless, for almost all measurements, the Picarro G2508 shows higher fluxes than the fast-box fluxes, especially when fluxes were relatively high (Figure 29).

4 Conclusion

4.1 Method comparison

The unique set-up of the experiment allowed comparison of all three methods. All methods show peak N_2O emissions during events related to agricultural management, but variation in the flux resulted in relative large differences in the cumulative emission due to several factors. Despite these differences, the cumulative emission was still largely within the range of several studies with similar experiments. Furthermore, each method has its own advantage and disadvantage, and all methods can complement each other for a deeper insight on the effect of grassland renewal on GHG emissions.

4.2 Eddy Covariance conclusive

In principle, flux measurements of CO_2 and N_2O using the Eddy-Covariance (EC) technique can be conducted sequentially on three different fields. Using long inlet lines is possible but require an intensive flux damping analysis. Since fields were close to each other, footprints had contributions from at least two flux contributors with their individual vegetation and surface roughness leading to unique (co)spectra, which are probably not represented by theoretical spectra sufficiently. An aera weighting approach was applied to extract the individual field contributions from the measured flux assuming that the flux scales with the area and fluxes outside fields can be approximated by fluxes from the reference field. The scaling can be prevented by using larger fields, but then also larger inlet lines are needed, which makes the damping corrections more difficult - if still possible.

Fluxes of CO_2 seem reasonable and carbon budget calculation using common gap-filling approaches was possible even with a “low” amount of high-quality data. From the perspective of EC measurement community, we only have 1200-1300 measurements over the 180 days of the campaign. This is however a big step forward compared to our chamber measurements where we have in the order of 150 measured emissions per field.

Final budgets were obtained by area scaling which is needed because the Eddy Covariance technique does not only show the effect of one field but can show a combination of the fields in which the sample is taken and the adjacent fields. These corrections by aera weighting were higher for the wheat and grass field than for the reference field. The reason for that is that these fields were smaller and thus have more effect from the adjacent fields.

Apart from the ploughing and fertilizing periods the N_2O exchange was close to zero. N_2O fluxes were in the range of ± 36 µg N m^{-2} h^{-1} making the estimation of reliable N_2O budgets challenging using statistical gap-filling methods. Since N_2O fluxes have a large variability, application of statistical gap-filling methods may introduce a large uncertainty. Thus, we tried a novel machine learning algorithm – a random forest (RF) approach. Using the RF approach, N_2O budgets of the wheat and grass field were similar and by the factor 2.9 to 4 larger than the reference field in case of the application of area weighting.

Fluxes from chamber measurements predicted lower values by a factor ranging from 2.2 to 2.9 for the managed fields, which is still in a reasonable range. The discrepancy between EC and chamber fluxes was largest for the reference field.

For further applications of this measurement setup, we suggest to choose fields with similar dimensions to the reference field, but this requires longer inlet lines as written above. Continuous arrangements of the measurement height may also be considered for the best footprint coverage. An increase in the data coverage may be needed for N_2O improving the robustness of the gap-filling issue but it requires a reduction in fields included in the setup. Generally, an increase in sampling frequency to 10 Hz may also enhance data quality, which requires to neglect certain compounds from measuring. Additional high to modest frequency measurements of biological, meteorological, and soil parameters are recommended for data calculation and interpretation.

4.3 Effect of grassland renewal on GHG emissions

Grassland management is identified as the highest potential measure for carbon sequestration due to its large area of grassland in the Netherlands to achieve the goal that was set in the Dutch Climate Accord of 2019. In terms of carbon storage and climate mitigation, we conclude that permanent grassland would be the preferred option over conversion to arable land and grassland renewal as permanent grassland was a sink for carbon. However, grassland renewal is considered important to maintain the yield and nutritional value of the grass, as well as to keep up other ecosystem services related to grass production, such as soil quality. This study show that that periodical grassland renewal does not lead to C loss at the end of the experimental period. In fact, the measurement period was only four months and, in that time, the temporary loss of C was already compensated. Continuing the experiment could result in carbon sequestration on the longer term. Conversion to arable land result in a net C loss. N_2O- emission was lowest for reference overall, but for reseeded and wheat the results are not in agreement throughout all three methods. Nevertheless, in terms of CO_2-eq, permanent grassland is the preferred option over grassland renewal and conversion to arable land.

5 References

Aubinet, M., Vesala, T., and Papale, D., eds. (2012) Eddy Covariance: A Practical Guide to Measurement and Data Analysis, Springer Science+Business Media B.V. 2012, 438 pp., https://doi.org/10.1007/978-94-007-2351-1.

Bajgain, R., Xiao, X., Basara, J., Wagle, P., Zhou, Y., Mahan, H., Gowda, P., McCarthy, H. R., Northup, B., Neel, J., and Steiner, J. (2018) Carbon dioxide and water vapor fluxes in winter wheat and tallgrass prairie in central Oklahoma, 644, 1511-1524, https://doi.org/10.1016/j.scitotenv.2018.07.010.

Biegemann, T., 2014. Grünlandumbruch und Neuansaat: kurz- und langfristige Effekte auf Treibhausgasemissionen und Ertragsleistungen von Grünlandbeständen. Dissertation. Institut für Pflanzenbau und Pflanzenzüchtung, Christian-Albrechts-Universität zu Kiel (in German)

Buchen, C., Well, R., Helfrich, M., Fuß, R., Kayser, M., Gensior, A., Benke, M., Flessa, H., 2017. Soil mineral N dynamics and N2O emissions following grassland renewal. Agric. Ecosyst. Environ. 246, 325–342

Burba, G. (2013) Eddy Covariance Method for Scientific, Industrial, Agricultural and Regulatory Applications: A Field Book on Measuring EcosystemGas Exchange and Areal Emission Rates, LI-COR Biosciences.

Cardenas, L. M., Olde, L., Loick, N., Griffith, B., Hill, T., Evans, J., Cowan, N., Segura, C., Sint, H., Harris, P., McCalmont, J., Zhu, S., Dobermann, A., and Lee, M. R. F. (2022) CO_2 fluxes from three different temperate grazed pastures using Eddy covariance measurements, Science of The Total Environment, 831, 154819, https://doi.org/10.1016/j.scitotenv.2022.154819.

Cowan, N. J., Levy, P. E., Famulari, D., Anderson, M., Drewer, J., Carozzi, M., Reay, D. S., and Skiba, U. M. (2016) The influence of tillage on N_2O fluxes from an intensively managed grazed grassland in Scotland, Biogeosciences, 13, 4811–4821, https://doi.org/10.5194/bg-13-4811-2016.

Cowan, N., Levy, P., Maire, J., Coyle, M., Leeson, S. R., Famulari, D., Carozzi, M., Nemitz, E., Skiba, U. (2020) An evaluation of four years of nitrous oxide fluxes after application of ammonium nitrate and urea fertilisers measured using the eddy covariance method, Agricultural and Forest Meteorology, 280, 107812, https://doi.org/10.1016/j.agrformet.2019.107812.

Davies, M., Smith, K., Vinten, A., 2001. The mineralisation and fate of nitrogen following ploughing of grass and grass-clover swards. Biol. Fertil. Soils 33, 423–434

Falge, E., Baldocchi, D., Olson, R., Anthoni, P., Aubinet, M., Bernhofer, C., Burba, G., Ceulemans, R., Clement, R., Dolman, H., Granier, A., Gross, P., Grünwald, T., Hollinger, D., Jensen, N.-O., Katul, G., Keronen, P., Kowalski, A., Lai, C. T., Law,
B. E., Meyers, T., Moncrieff, J., Moors, E., Munger, J., Pilegaard, K., Üllar Rannik, Rebmann, C., Suyker, A., Tenhunen, J., Tu, K., Verma, S., Vesala, T., Wilson, K., and Wofsy, S. (2001) Gap filling strategies for defensible annual sums of net ecosystem exchange, Agricultural and Forest Meteorology, 107, 43–69, https://doi.org/10.1016/S0168-1923(00)00225-2.

Finkelstein, P. L. and Sims, P. F. (2001) Sampling error in eddy correlation flux measurements, J. Geophys. Res., 106, 3503–3509, https://doi.org/10.1029/2000JD90073.

M. Helfrich, G. Nicolay,R. Well, C. Buchen-Tschiskale, R. Dechow, R. Fuß, A. Gensior, H. Marten Paulsen, C. Berendonk, H. Flessa. (2020). Effect of chemical and mechanical grassland conversion to cropland on soil mineral N dynamics and N_2O emission. Agriculture, ecosystems & environment, 298, 106975. doi: 10.1016/j.agee.2020.106975

Ibrom, A., Dellwick, E., Flyvbjerg, H., Jensen, N. O., and Pilegaard, K.: Strong low-pass filtering effects on water vapour flux measurements with closed-path eddy correlation systems, Agr. Forest Meteorol., 147, 140–156, https://doi.org/10.1016/j.agrformet.2007.07.007, 2007.

Kayser, M., Müller, J., & Isselstein, J. (2018). Grassland renovation has important consequences for C and N cycling and losses. Food and Energy Security, 7(4).

Kljun, N., Calanca, P., Rotach, M. W., and Schmid, H. P. (2015) A simple two-dimensional parameterisation for Flux Footprint Prediction (FFP), Geosci. Model Dev., 8, 3695-3713, https://doi.org/10.5194/gmd-8-3695-2015.

Langford, B., Acton, W., Ammann, C., Valach, A., and Nemitz, E.: Eddy-covariance data with low signal-to-noise ratio: time-lag determination, uncertainties and limit of detection, Atmos. Meas. Tech., 8, 4197–4213, https://doi.org/10.5194/amt-8-4197-2015, 2015.

Liang, L. L., Campbell, D. I., Wall, A. M., Schipper, L. A. (2018) Nitrous oxide fluxes determined by continuous eddy covariance measurements from intensively grazed pastures: Temporal patterns and environmental controls, Agriculture, Ecosystems & Environment, 268,171-180, https://doi.org/10.1016/j.agee.2018.09.010.

Lognoul, M., Debacq, A., De Ligne, A., Dumont, B., Manise, T., Bodson, B., Heinesch, B., and Aubinet, M. (2019) N_2O flux short-term response to temperature and topsoil disturbance in a fertilized crop: An eddy covariance campaign,
Agricultural and Forest Meteorology, 271, 193-306, https://doi.org/10.1016/j.agrformet.2019.02.033.

Mahabbati, A., Beringer, J., Leopold, M., McHugh, I., Cleverly, J., Isaac, P., and Izady, A. (2021) A comparison of gap-filling algorithms for eddy covariance fluxes and their drivers, Geosci. Instrum. Method. Data Syst., 10, 123–140, https://doi.org/10.5194/gi-10-123-2021.

Mammarella, I., Launiainen, S., Gronholm, T., Keronen, P., Pumpanen, J., Rannik, U., and Vesala, T. (2009) Relative Humidity Effect on the High-Frequency Attenuation of Water Vapor Flux Measured by a Closed-Path Eddy Covariance System, J. Atmos. Ocean. Tech., 26, 1856–1866, https://doi.org/10.1175/2009JTECHA1179.1.

Mauder, M. and Foken, T. (2006) Impact of post-field data processing on eddy covariance flux estimates and energy balance closure. Meteorologische Zeitschrift, 15: 597-609.

Moncrieff, J. B., Massheder, J. M., de Bruin, H., Ebers, J., Friborg, T., Heusinkveld, B., Kabat, P., Scott, S., Soegaard, H., and Verhoef, A. (1997) A system to measure surface fluxes of momentum, sensible heat, water vapor and carbon dioxide. Journal of Hydrology, 188-189: 589-611, https://doi.org/10.1016/S0022-1694(96)03194-0.

Moncrieff, J. B., Clement, R., Finnigan, J., and Meyers, T. (2004) Averaging, detrending and filtering of eddy covariance time series, in Handbook of micrometeorology: a guide for surface flux measurements, eds. Lee, X., Massman, W. J., and Law, B. E. Dordrecht: Kluwer Academic, 7-31.

Moore, C. J. (1986). Frequency response corrections for eddy correlation systems. Boundary-Layer Meteorology, 37: 17-35, https://doi.org/10.1007/BF00122754.

Nakai, T., K. Shimoyama. (2012) Ultrasonic anemometer angle of attack errors under turbulent conditions. Agricultural and Forest Meteorology, 18: 162-163, https://doi.org/10.1016/j.agrformet.2012.04.004.

Murphy, R. M., Saunders, M., Richards, K. G., Krol, D. J., Gebremichael, A. W., Rambaud, J., Cowan, N., and Lanigan, G. J. (2022) Nitrous oxide emission factors from an intensively grazed temperate grassland: A comparison of cumulative emissions determined by eddy covariance and static chamber methods,
Agriculture, Ecosystems & Environment, 324, 107725, https://doi.org/10.1016/j.agee.2021.107725.

Oertel, C., Matschullat, J., Zurba, K., Zimmermann, F., Erasmi, S. (2016). Greenhouse gas emissions from soils – A review. Elsevier, Chemie der Erder 76 (2016), 327-352.

Pedregosa, F.,Varoquaux, G., Gramfort, A., Michel, V., Thirion, B., Grisel, O., Blondel, M., Prettenhofer, P., Weiss, R., Dubourg, V., Vanderplas, J., Passos, A., Cournapeau, D., Brucher, M., Perrot, M., and Duchesnay, É (2011) Scikit-learn: Machine Learning in Python, 12, 2825–2830, http://jmlr.org/papers/v12/pedregosa11a.html.

Rebmann, C., Aubinet, M., Schmid, H. P., Arriga, N., Aurela, M., Burba, G., Clement, R., De Ligne, A., Fratini, G., Gielen, B., Grace, J., Graf, A., Gross, P., Haapanala, S., Herbst, M., Hörtnagl, L., Ibrom, A., Joly, L., Kljun, N., Kolle, O., Kowalski, A., Lindroth, A., Loustau, D., Mammarella, I., Mauder, M., Merbold, L., Metzger, S., Mölder, M., Montagnani, L., Papale, D., Pavelka, M., Peichl, M., Roland, M., Serrano-Ortiz, P., Siebicke, L., Steinbrecher, R., Tuovinen, J.-P., Vesala, T., Wohlfahrt, G., and Franz, D. (2018) ICOS eddy covariance flux-station site setup: a review, Int. Agrophys., 32, 471–494, https://doi.org/10.1515/intag-2017-0044.

Reichstein, M., Falge, E., Baldocchi, D., Papale, D., Aubinet, M., Berbigier, P., Bernhofer, C., Buchmann, N., Gilmanov, T., Granier, A., Grünwald, T., Havránková, K., Ilvesniemi, H., Janous, D., Knohl, A., Laurila, T., Lohila, A., Loustau, D., Matteucci, G., Meyers, T., Miglietta, F., Ourcival, J.-M., Pumpanen, J., Rambal, S., Rotenberg, E., Sanz, M., Tenhunen, J., Seufert, G., Vaccari, F., Vesala, T., Yakir, D., and Valentini, R. (2005) On the separation of net ecosystem exchange into assimilation and ecosystem respiration: review and improved algorithm, Glob. Change Biol., 11, 1424–1439, https://doi.org/10.1111/j.1365-2486.2005.001002.x.

Reinsch, T., Loges, R., Kluß, C., Taube, F., 2018. Renovation and conversion of permanent grass-clover swards to pasture or crops: effects on annual N2O emissions in the year after ploughing. Soil Till. Res. 175, 119–129

Schmidt, M., Reichenau, T. G., Fiener, P., and Schneider, K. (2012) The carbon budget of a winter wheat field: An eddy covariance analysis of seasonal and inter-annual variability, Agricultural and Forest Meteorology, 165, 114-126, https://doi.org/10.1016/j.agrformet.2012.05.012.
Su, H.-B., Schmid, H. P., Grimmond, C. S. B., Vogel, C. S., and Oliphant, A. J. (2004) Spectral characteristics and correction of long-term eddy-covariance measurements over two mixed

hardwood forests in non-flat terrain, Bound.-Lay. Meteorol., 110, 213–253, https://doi.org/10.1023/A:1026099523505.

Velthof, G. and Oenema, O. (1995) Nitrous oxide fluxes from grassland in the Netherlands: I. Statistical analysis of flux-chamber measurements. European Journal of Soil Science, 46, 533-540. https://doi.org/10.1111/j.1365-2389.1995.tb01349.x

Velthof, G. L., Hoving, I. E., Dolfing, J., Smit, A., Kuikman, P. J., & Oenema, O. (2010). Method and timing of grassland renovation affects herbage yield, nitrate leaching, and nitrous oxide emission in intensively managed grasslands. Nutrient Cycling in Agroecosystems, 86, 401–412. https://doi.org/10.1007/s10705-009-9302-7

Velthof, G.L., Jarvis, S. C., Stein, A., Allen, A. G., Oenema, O. (1996) Spatial variability of nitrous oxide fluxes in mown and grazed grasslands on a poorly drained clay soil, Soil Biology and Biochemistry, 28, 1215-1225, https://doi.org/10.1016/0038-0717(96)00129-0.

Vickers, D. and Mahrt, L. (1997) Quality control and flux sampling problems for tower and aircraft data. Journal of Atmospheric and Oceanic Technology, 14: 512-526, https://doi.org/10.1175/1520-0426(1997)014<0512:QCAFSP>2.0.CO;2.

Wilczak, J. M., Oncley, S. P. and Stage, S. A. (2001). Sonic anemometer tilt correction algorithms. Boundary-Layer Meteorology, 99: 127-150, https://doi.org/10.1023/A:1018966204465.

Wintjen, P., Ammann, C., Schrader, F., and Brümmer, C. (2020) Correcting high-frequency losses of reactive nitrogen flux measurements, Atmos. Meas. Tech., 13, 2923–2948, https://doi.org/10.5194/amt-13-2923-2020.

Wutzler, T., Lucas-Moffat, A., Migliavacca, M., Knauer, J., Sickel, K., Šigut, L., Menzer, O., and Reichstein, M. (2018) Basic and extensible post-processing of eddy covariance flux data with REddyProc, Biogeosciences, 15, 5015–5030, https://doi.org/10.5194/bg-15-5015-2018.

Zhu, S., Clement, R., McCalmont, J., Davies, C. A., and Hill, T.: Stable gap-filling for longer eddy covariance data gaps (2022) A globally validated machine-learning approach for carbon dioxide, water, and energy fluxes, Agricultural and Forest Meteorology, 314, 108777, https://doi.org/10.1016/j.agrformet.2021.108777

6 Appendix

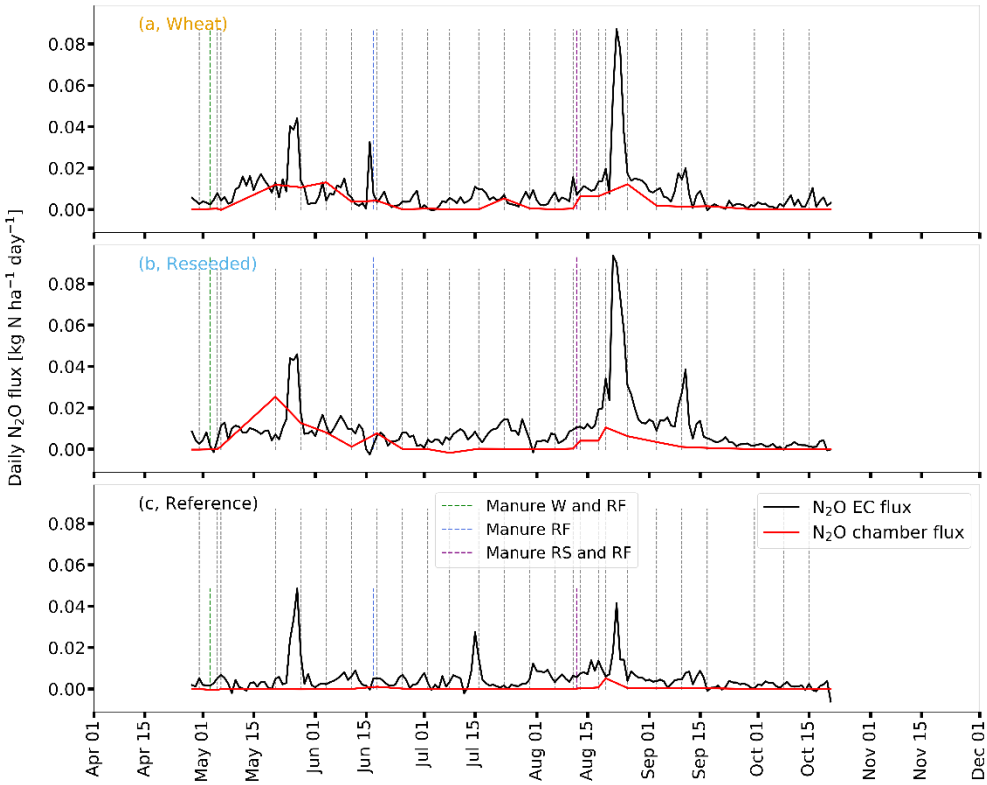

Supporting Figure S1: Comparison of flux chamber measurements (red) and gap-filled EC flux time series (black) of N_2O shown as daily averages for each field in kg N ha^{-1} day^{-1}.

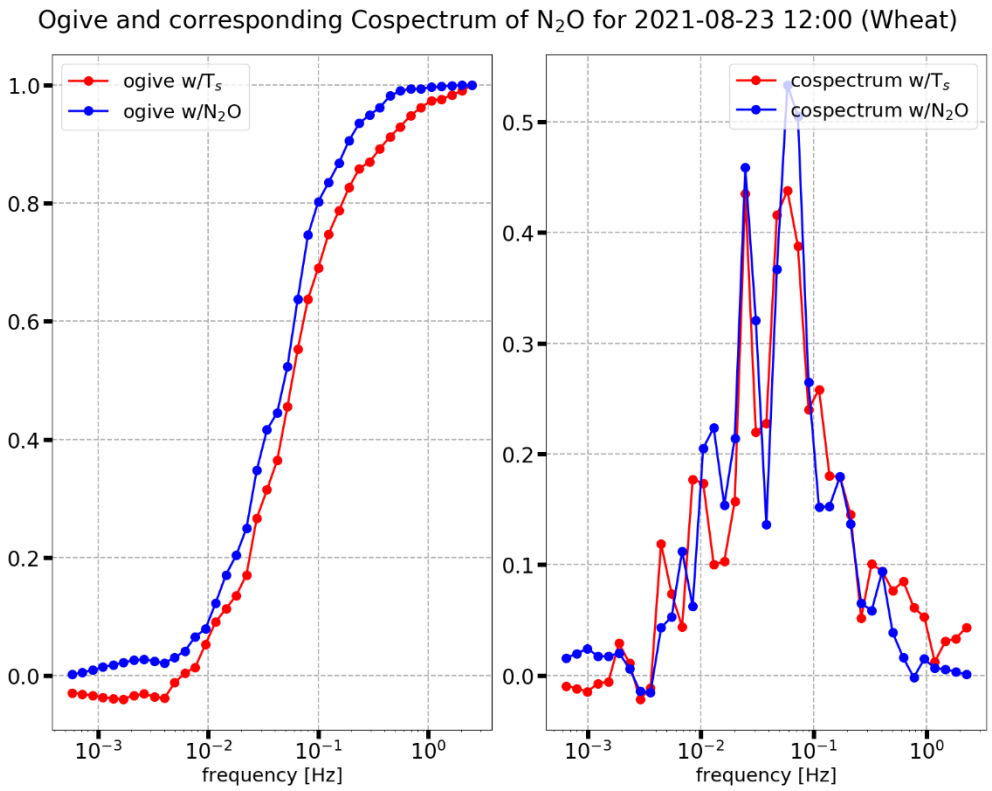

Supporting Figure S2 Ogive (right) and cospectrum (left) of N_2O (blue) for a certain half-hourly flux. Sensible heat ogive and cospectrum are coloured red. Spectral data were binned into log-spaced frequency data points.

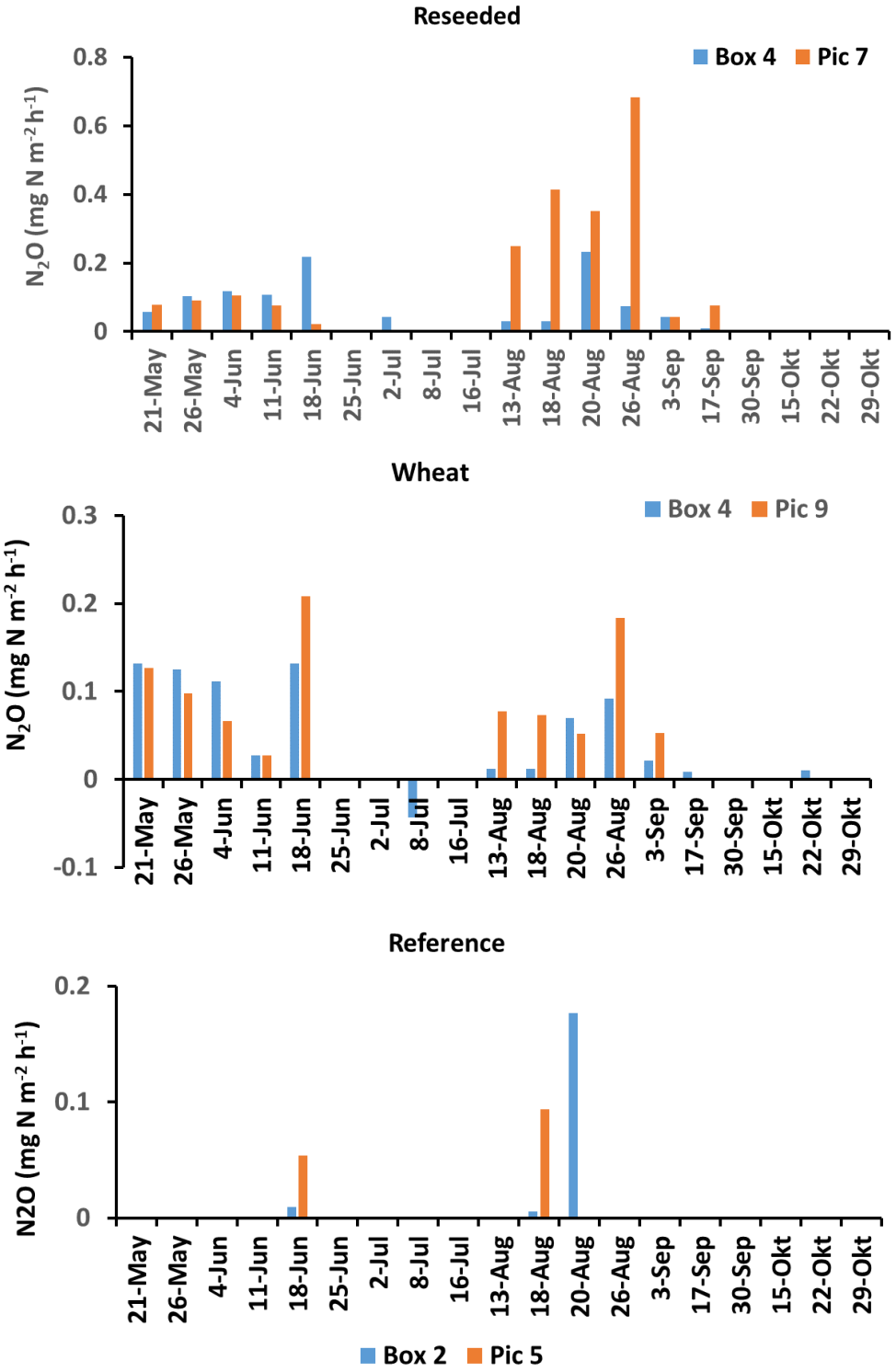

Supporting Figure S3: flux data of individual fast-box and static chamber measurement on the exact same location on each treatment.

Supporting Table S1: Physical parameters of the EC installation.

	Field Wheat	Field Reseeded	Field Reference5	
Measurement height	1.9 m	1.9 m	1.9 m	
Sonic Anemometer	Gill Windmaster Pro, Firmware: 2329-701			
North alignment	Spar			
North Offset	0°			
Tube length	93.7 m	96.2 m	90.0 m	12.8 m
Tube inner diameter	4.3 mm			
Flow rate	5.6 L min^{-1}	4.3 L min^{-1}	5.0 L min^{-1}	
Northward sep.	0.0 cm	0.0 cm	0.0 cm	
Eastward sep.	0.0 cm	0.0 cm	0.0 cm	
Vertical sep.	-17.0 cm	-17.0 cm	-17.0 cm	
Longitudinal path length	20.0 cm	20.0 cm	20.0 cm	
Lateral path length	4.0 cm	4.0 cm	4.0 cm	
Time response	0.3 s	0.3 s	0.3 s	
Minimum time lag	7.0 s	7.0 s	7.0 s	0.0 s
Default time lag	15.0	15.0	15.0 s	2.0 s
Maximum time lag	23.0 s	23.0 s	23.0 s	8.0 s

Energy & Materials Transition

Westerduinweg 3
1755 LE Petten
www.tno.nl

TNO innovation for life